People`s Democratic Republic of Algeria

Ministry of Higher Education and Scientific Research

University of Echahid Hamma Lakhdar - El Oued

Faculty of Technology

Department of Mechanical engineering

Dissertation

ACADEMIC MASTER

Domain: Science and Technology

Division: Electromecanic

Specialty: Electromecanic

Presented by:

1. BEDDA ZEKRI Ziad
2. GUERFI Djamal Eddine
3. MERAGHNI Abdelhai

Entitled:

An advanced control of dual three-phase induction motor

Publicly defended in: 29/05/2025

Board of Examiners:

Dr. ABDELKRIM MOHREM	**Chairman**
Dr. HAMZA MESAI AHMED	**Supervisor**
Dr. MOHAMMED SACI CHABANI	**Examiner**

Academic Year: 2024/2025

Abstract:

Multiphase machines have gained significant attention in modern high-power applications due to their enhanced reliability and flexibility in power distribution. Among them, the dual three-phase induction machine presents notable advantages, as it incorporates two sets of three-phase windings within a single stator and is typically powered by dual voltage inverters. Recent research trends emphasize the integration of artificial intelligence techniques to boost the effectiveness and robustness of control strategies. This thesis focuses on the simulation-based analysis of field-oriented control based on the artificial neural networks (ANN-FOC) applied to a dual three-phase induction machine.

Key words:

Multiphase machines, Dual three-phase induction machine, Field-oriented control (FOC), PI Controllers, ANN controllers.

Résumé:

Les machines multiphases suscitent un intérêt croissant dans les applications à haute puissance, notamment grâce à leur fiabilité améliorée et leur aptitude à la distribution segmentée de la puissance. La machine asynchrone triphasées à double alimentation se distingue par la présence de deux groupes d'enroulements triphasés identiques intégrés dans un même stator, alimentés par deux convertisseurs de tension distincts. Les recherches récentes mettent en évidence l'apport des techniques d'intelligence artificielle pour optimiser l'efficacité et la robustesse de techniques de commande. Ce travail propose une étude par simulation de la commande vectorielle basée sur les réseaux de neurone artificiel (ANN-FOC) appliquée à une machine asynchrone double triphasées.

Mots clés:

Machines multiphases, Machine asynchrone triphasées à double alimentation, Commande vectorielle (FOC), Régulateurs PI , Régulateurs ANN.

الملخص:

شهدت الآلات متعددة الأطوار اهتمامًا متزايدًا في التطبيقات الكهربائية عالية القدرة، بفضل موثوقيتها العالية وقدرتها على توزيع الطاقة بشكل أكثر مرونة. وتُعد آلة الحث ثلاثية الأطوار مزدوجة التغذية من أبرز هذه الآلات، حيث تحتوي على مجموعتين من اللفات الثلاثية موضوعة داخل نفس الجزء الثابت، ويتم تشغيلها بواسطة محولين للجهد. تُؤكد أحدث اتجاهات البحث على أهمية دمج تقنيات الذكاء الاصطناعي لتعزيز فعالية استراتيجيات التحكم ومتانتها. تُركز هذه الأطروحة على التحليل القائم على المحاكاة للتحكم الميداني، استنادًا إلى الشبكات العصبية الاصطناعية (ANN–FOC)، والمُطبق على آلة حث ثنائية ثلاثية الطور.

كلمات مفتاحية :

آلات متعددة الأطوار، آلة الحث ثلاثية الأطوار مزدوجة التغذية، التحكم الموجه ميدانيًا (FOC)، منظمات PI، منظمات ANN.

Dedication

We dedicate this work to our beloved families for their constant support, encouragement, and sacrifices throughout our academic journey.

We also extend our deepest appreciation to our supervisors and professors for their valuable guidance and assistance.

Finally, we dedicate this work to all our friends and colleagues who have supported us along the way.

Acknowledgments

*We begin by expressing our heartfelt thanks to **ALLAH** for granting us the strength and determination to complete this work.*

*We are deeply grateful to our supervisor, **Dr. Mesai Ahmed Hamza**, for his continuous support, enthusiasm, and insightful guidance throughout the course of this project.*

We would also like to sincerely thank the jury members for taking the time to evaluate our work.

Finally, we extend our appreciation to everyone who contributed, in one way or another, to the successful completion of this study.

List of figures:

List of tables

SYMBOLS:

- Modeling Parameters of dual three phase IM **:**

R_s	(Ω)	Stator resistance per phase,
R_r	(Ω)	Rotor resistance per phase,
L_s	(H)	Stator cyclic inductance by phase,
L_r	(H)	Rotor cyclic inductance per phase,
L_m	(H)	Mutual cyclic inductance (between stator and rotor), magnetizing inductance,
l_s	(H)	Specific inductance of a statoric phase,
l_r	(H)	Clean inductance of a rotor phase,
m_s	(H)	Mutual inductance between two stator phases,
m_r	(H)	Mutual inductance between two rotor phases,
M	(H)	Maximum value of mutual inductance between stator phase and other rotoric phase,
p	(–)	number of pole pairs,
C_{em}	(N.m)	Electromagnetic torque of the generator

- **Reference Frames:**

(s_a, s_b, s_c)	Magnetic axes linked to three-phase stator windings,
(r_a, r_b, r_c)	Magnetic axes linked to three-phase rotor windings,
(dq_1), (dq_2)	Park reference axes,
($\alpha\beta_1$), ($\alpha\beta_2$)	Concordia/Clarke reference axes,
θ_{sr} (rad)	Rotor angular position relative to stator,
θ_s (rad)	Stator angular position relative to axis (d).
θ_r (rad)	Rotor angular position relative to axis (d).

- **Electrical quantities :**

$v_{s\ abc1}$, $v_{s\ abc2}$	(V)	Three Phase Instantaneous Stator Voltages,
$v_{r\ a,\ b,\ c}$	(V)	Three Phase Instantaneous Stator Voltages,
$v_{s\ dq1}$, $v_{s\ dq2}$	(V)	Two-phase stator voltages in landmark (d, q),
v_{rdq}	(V)	Two-phase stator voltages in landmark (d, q),
V_s	(V)	Stator Voltage Vector Module,
$i_{s\ abc1}$, $i_{s\ abc2}$	(A)	Three Phase Stator Instantaneous Currents,
$i_{r\ abc}$	(A)	Three Phase Stator Instantaneous Currents,
$i_{s\ dq1}$,$i_{s\ dq2}$	(A)	Two-phase stator currents in landmark (d, q),
i_{rdq}	(A)	Two-phase stator currents in landmark (d, q),
$\phi_{s\ abc1}$, $\phi_{s\ abc2}$	(Wb)	Instant Magnetic Flow to Stator,

$\phi_{s\,dq1}$, $\phi_{s\,dq2}$	(Wb)	Two-phase stator flows in the rotating landmark (d, q).
Ψ_s	(Wb)	Stator flux vector module.
$\phi_{r\,ab\,c}$	(Wb)	Rotor magnetic flux vector,
ϕ_{rdq}	(Wb)	Two-phase rotor flows in the rotating landmark (d, q).
Ψ_r	(Wb)	Rotor Flux Vector Module.
P_s	(W)	Stator Active Power,
Q_s	(VAr)	Stator reactive power.
$P_{réseau}$	(W)	Power supplied to the network,

- **Mechanical quantities :**

ω_r	(rad/s)	Electric pulse corresponding to the speed of rotation,
ω_s	(rad/s)	Electric pulsation of stator quantities (rotating field),
G	(–)	Rotation speed shift,
f_s	(Hz)	Electrical frequency of stator quantities,
f_r	(Hz)	Electrical frequency of rotor quantities,
N_s	(tr/min)	Speed of the rotating field,

- **Transformations :**

s	Laplace operator,
$P(\theta)$	Park Transformation:$X_{sa,b,c} \rightarrow X_{sd,q}$ et$X_{ra,b,c} \rightarrow X_{rd,q}$,

- **Control quantities of the D3PH-IM :**

K_p, K_i	(–)	Proportional and integral components of the PI corrector,
r	(–)	Modulation rate (adjustment index),
m	(–)	modulation index,
f_r	(Hz)	reference frequency,
w_i	(–)	Weight vector
η_i	(–)	learning rate
ψ_i,ϕ_i,	(–)	vector-valued functions
P_i	(–)	Predicate error
H_i	(–)	Matrix gradient
Q_i, R_i	(–)	matrices de covariance
S	(–)	Fonction de limite
α, β	(–)	Constant values

NOTATIONS:

D3PH-IM	: Dual three phase induction machine.
MSC	: Machine Side Converter.
CVI	: Indirect Vector Control.
MCC	: Machine à Courant Continu.
PWM	: Pulse Width Modulation.
PI	: Proportional Integral.

AC	: Alternatif Current.
DC	: Direct Current.
FOC	: Field Oriented Control.
ANN	: Artificial Neural Networks.
RNN	: Recurrent Neural Networks.
EKF	: Extended KalmanFilter .
MPC	: Model Predictive Control
PCC	: Predictive Current Control
MB-PCC	: Model-Based Predictive Current Control
MF-PCC	: Model-Free Predictive Current Control
MPPT	: Maximum Power Point Tracking.
MLP	: Multi Layer Perceptron.
IGBT	: Insulated Gate Bipolar Transistor.
NPC	: Neutral Point Clamped.
WECS	: Wind Energy Conversion Systems.

General Introduction

In recent years, alternating current (AC) machines powered by static converters have seen growing adoption in high-power industrial sectors. However, the performance of such systems is often constrained by the limitations of the power semiconductor devices, especially in terms of switching frequency. To overcome these constraints, power segmentation has emerged as a practical solution. It enables the use of higher switching frequency components, while ensuring that the electric machines can deliver reliable performance in high-power applications such as railway traction, marine propulsion, and large-scale wind energy conversion systems.

One effective approach to power segmentation is the use of multiphase machines—machines equipped with more than the traditional three phases. Among these, dual three-phase induction machine is a particularly compelling configuration. This topology offers several key advantages over its three-phase counterparts, including reduced per-phase current, improved torque density, and enhanced fault tolerance. Moreover, it allows continued operation under faulted conditions, making it highly suitable for critical applications where reliability is paramount.

Historically, multiphase machines date back to the 1920s when they were introduced to segment the power of electrical generators. Today, they are poised to play a significant role in the realm of high-performance variable speed drives. In particular, six-phase asynchronous machines are increasingly being considered in advanced drive systems due to their mechanical robustness, thermal reliability, and capacity to minimize low-frequency torque ripples.

Despite their advantages, dual three-phase induction machines come with inherent challenges. The control of dual three-phase -IMs is more complex due to their nonlinear dynamic behavior and the strong coupling between internal variables such as rotor flux and electromagnetic torque. This complexity necessitates advanced control strategies and precise modeling techniques to fully exploit the benefits of these machines.

This thesis is structured into four chapters that collectively explore the modeling, control, and performance optimization of the dual three-phase induction machine using multi-level inverters:

- **Chapter 1** presents an overview of multiphase machines, focusing on the challenges and motivations behind their use, and introducing the Double-star asynchronous machine as the central focus of this study.
- **Chapter 2** is dedicated to the modeling of the dual three-phase induction machine and its associated power supply, which consists of two PWM-controlled voltage inverters. This chapter also covers rotor flux orientation control under both nominal and disturbed operating conditions.
- **Chapter 3** delves into vector control strategies, particularly rotor flux-oriented control (FOC) applied to the dual three-phase induction machine with two-level inverters. It includes simulation-based performance evaluations under varying operating conditions.
- **Chapter 4** explores the use of artificial neural networks to further enhance the control robustness and performance of dual three-phase induction machines. This includes a comparative analysis of classical and intelligent vector control, focusing on torque performance, current ripple reduction, and robustness against parameter variations.

Finally, a general conclusion will summarize the key findings of this work and provide insights into future research directions.

CHAPTER I

Multiphase machines: overview, challenges, and context of study

I.1 Introduction:

Among the wide range of electric motors, induction motors have maintained their popularity for over a century. Their widespread use in industrial applications is largely due to their durability, low manufacturing cost, and minimal maintenance requirements, making them a preferred choice over DC and other AC motors. A recent area of research in induction motor drives is the implementation of multiphase induction machines, where the stator includes more than three phases.

In this chapter, we begin with a brief historical background of electrical machines. Then, we introduce multiphase machines, outlining their main characteristics, operating principles, as well as the benefits and limitations associated with their use in various applications. Lastly, we provide an overview of dual three phase induction machines powered by multi-level inverters.

I.2 General overview of multi-phase machines:

I.2.1 Evolution of multi-phase machines:

The development of multiphase electrical machines has evolved from the foundations of classical three-phase systems. The concept of using more than three phases was first explored in the early 20th century to address the limitations of traditional machines in high-power applications. The initial use of multiphase systems dates back to the 1920s, when large-scale alternators in power stations adopted multi-phase windings such as six-phase stators to enhance power handling and improve fault tolerance.

Significant theoretical advancements occurred in the 1960s and 1970s, as researchers began exploring the mathematical modeling of multiphase systems and their advantages in specialized industrial environments. During this period, interest grew in the use of five-phase and six-phase induction machines for railway traction and aerospace propulsion, driven by the potential for smoother torque production and reduced harmonic content.

The 1990s marked a turning point with the advent of high-speed digital controllers and power electronics, allowing real-time control of machines with more than three phases. This enabled the development of vector control strategies tailored specifically for multiphase systems, expanding their use in electric vehicles, wind turbines, and fault-tolerant applications.

In recent years, the multiphase motor concept has been further refined. Researchers have demonstrated that increasing the number of phases enhances system redundancy, enables

better fault operation under phase loss, and improves overall system reliability. As a result, dual three-phase (D3PH) and other high-phase-order machines are increasingly favored in safety-critical and high-performance domains such as aviation and electric naval propulsion systems [1].

I.2.2 Systematic classification of multi-phase machines:

Multi-phase machines are defined by their number of stator phases more than the conventional three and are categorized based on configuration and application. Their unique structure offers enhanced performance and flexibility in control.

a) Classification based on phase number and winding structure:

Multiphase machines can be classified according to the number of stator phases:

- Five-phase and six-phase machines:
  - Most commonly used due to a balance between complexity and performance.
  - Suitable for applications requiring improved fault tolerance and torque quality.
- Higher-order phase machines (≥7 phases):
  - Typically used in experimental or highly specialized systems.
  - Offer additional degrees of freedom in control and fault isolation.

b) Classification based on structural design:

The core principles remain similar to traditional machines, but multiphase adaptations offer performance enhancements:

- Multiphase Induction Machines:
  - Utilize squirrel-cage or wound-rotor configurations
  - Preferred for ruggedness and simplicity in industrial drive systems
- Multiphase Synchronous Machines:
  - Can be designed with permanent magnets or field windings
  - Used in applications demanding high efficiency and precise speed control
- Dual Three-Phase Machines (D3PH):
  - Consist of two isolated three-phase windings spatially shifted
  - Support independent control of each subsystem, making them ideal for fault-tolerant drives and modular converter systems

Multiphase machines are especially valuable in applications requiring high reliability, such as aerospace actuators, offshore platforms, and electric traction, where continued operation during faults is critical [2].

I.3 Structural configuration of multi-phase machines:

Electric machines can be classified based on the type of electrical supply or their structural design. From a construction perspective, machines may be asynchronous with either a wound rotor or a squirrel-cage rotor, or synchronous with features such as permanent magnets, excitation windings, smooth or salient poles, and with or without damper windings. These machines can be supplied by current-source or voltage-source inverters.

Multiphase machines, as their name implies, operate similarly to conventional three-phase induction machines. They generally consist of two primary components:

- A **rotor**, which is a solid cylindrical element mounted on a shaft and typically equipped with interconnected windings.
- A **stator**, which is a stationary hollow cylinder housing multiple three-phase windings. These windings may be magnetically coupled or independent and are arranged in star (wye) formations. Each star set is typically fed by a dedicated static power converter. [3]

I.4 Characteristics of multi-phase machines:

Multiphase machines can be categorized based on the number of stator phases. When the number of phases is a multiple of three, two distinct types are generally identified: **Type 1** and **Type 2** multiphase machines. In practice, configurations with an even number of phases are rarely used unless that number is also a multiple of three.

For a given number of stator phases, various winding configurations are possible depending on the **angular offset** (α) between adjacent phase windings or phase groups. To clearly distinguish between these arrangements, the concept of the number of equivalent phases is introduced. It is defined by the relationship:

$$npha = \frac{\pi}{a} \qquad \text{(I.1)}$$

For example, a six-phase induction machine with an angular offset of $a = \frac{\pi}{6}$ between its star groups will exhibit different magnetic and electrical characteristics compared to a

machine with the same number of phases but a displacement of $= \frac{\pi}{3}$. These differences affect the machine's harmonic content, torque ripple, and fault tolerance behavior, making the angular arrangement a key design parameter [4][5].

I.4.1 Type 1 multi-phase machines:

In Type 1 multiphase machines, the number of stator phases is a multiple of three. These phases can be organized into η independent three-phase star groups, where η is a positive integer. This configuration allows the machine to maintain symmetrical phase groupings similar to conventional three-phase systems, which simplifies control and improves performance.

The relationship between the total number of stator phases η_{ph} and the number of star groups η is given by:

$$nph = 3\eta \ (\eta = 1,2,3\ldots.) \qquad \text{(I.2)}$$

This structure is commonly used due to its natural compatibility with standard three-phase control techniques and its balanced magnetic field distribution [4].

Number of phases (q)	Phase equivalent number ($\boldsymbol{qa}$)	Angular offset (a)	Schematic representation, position of the coils
3	3	$\boldsymbol{\frac{\pi}{3}}$	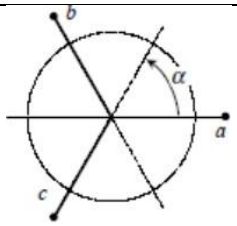
6	3	$\boldsymbol{\frac{\pi}{3}}$	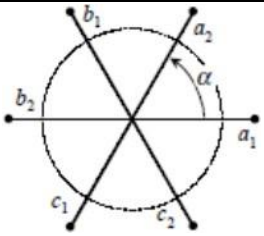
6	6	$\boldsymbol{\frac{\pi}{6}}$	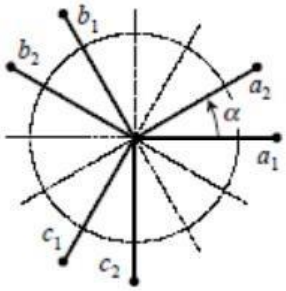

9	9	$\boldsymbol{\frac{\pi}{9}}$	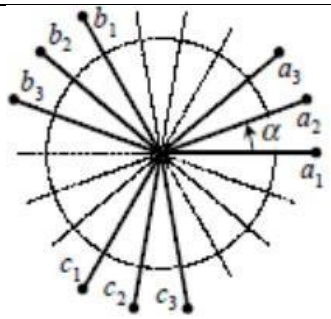
12	6	$\boldsymbol{\frac{\pi}{6}}$	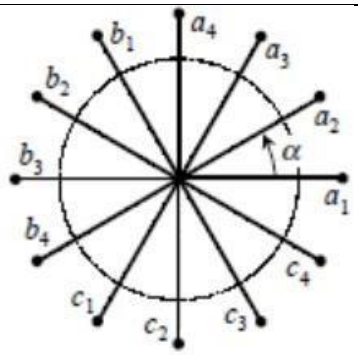
12	12	$\boldsymbol{\frac{\pi}{12}}$	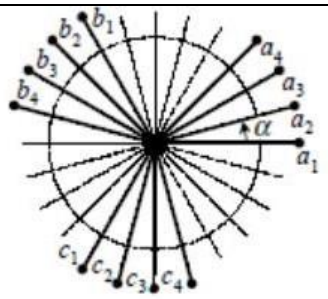

Table I.1: Machines with a number of stator phases multiple of three (Type 1).

I.4.2 Type 2 multi-phase machines:

This type are characterized by an odd number of stator phases that cannot be evenly divided into groups of three. These machines follow the general form:

$$nph = 3\eta+1 \ (\eta= 1,2,3\ldots.) \qquad \text{(I.3)}$$

Unlike Type 1 configurations, these machines have non-standard phase groupings, which can lead to unbalanced systems unless carefully managed. Despite the increased complexity, such configurations are sometimes used to improve fault tolerance or optimize specific electromagnetic performance criteria.

The angular displacement α between adjacent phase windings is generally defined as:

$$2a = \frac{2\pi}{nph} \qquad \text{so} \qquad nph = nph_a = \frac{\pi}{a} \qquad \text{(I.4)}$$

This confirms that the machine maintains a regular phase progression with uniform angular displacement, ensuring consistent electromagnetic torque production [4].

Number of phases (q)	Phase equivalent number ($\boldsymbol{qa}$)	Angular offset (a)	Schematic representation, position of the coils
5	**5**	$\frac{\boldsymbol{\pi}}{\boldsymbol{5}}$	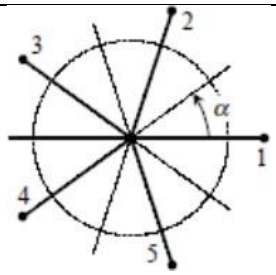
7	**7**	$\frac{\boldsymbol{\pi}}{\boldsymbol{7}}$	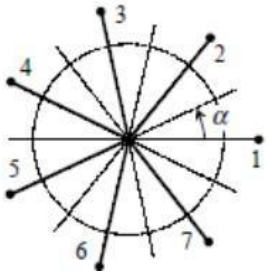
9	**9**	$\frac{\boldsymbol{\pi}}{\boldsymbol{9}}$	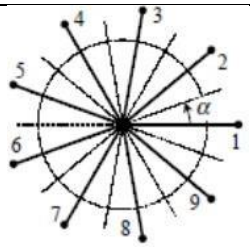
11	**11**	$\frac{\boldsymbol{\pi}}{\boldsymbol{11}}$	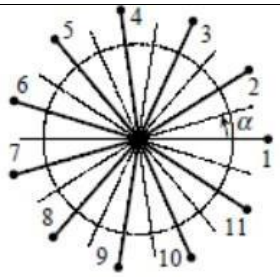
13	**13**	$\frac{\boldsymbol{\pi}}{\boldsymbol{13}}$	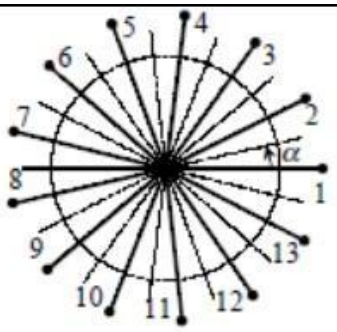

Table I.2: Machines with an odd number of stator phases (Type 2).

I.5 Operating principles of the multi-phase machine:

To illustrate the operating principle of a multiphase machine, consider a dual three-phase induction machine which is our case of study. In this configuration, the stator windings are divided into two sets of three-phase groups, commonly referred to as Star 1 and Star 2. These groups are supplied by three-phase currents of equal magnitude and frequency, with Star 2 shifted in phase by an angle α relative to Star 1. The interaction of these currents generates two rotating magnetic fields in the stator.

The rotational speed of the resulting magnetic field, known as the synchronous speed, depends on the supply frequency and the number of pole pairs. It is given by:

$$\omega_s = \frac{\mathbf{2\pi f}}{p} \quad [rad/s] \qquad \text{(I.5)}$$

where:

- ω_S is the synchronous speed,
- f is the supply frequency,
- p is the number of pole pairs.

These rotating stator fields induce electromotive forces (EMFs) and currents in the rotor conductors. As a result, the rotor begins to rotate at a speed ωr less than the synchronous speed ($\omega r <$). The difference in speed between the stator field and the rotor is referred to as the relative speed, defined by:

$$\omega = \omega_s - \omega r \qquad \text{(I.6)}$$

The slip, denoted by g , quantifies the relative difference between the synchronous and rotor speeds, and is expressed as:

$$g = \frac{\omega}{\omega s} = \frac{\omega s - \omega r}{\omega s} \qquad \text{(I.7)}$$

The operating mode of the machine depends on the value of the slip g. For instance, a slip close to zero indicates near-synchronous operation, typical of motors under steady-state conditions. A high slip value may occur during startup or under load changes [6].

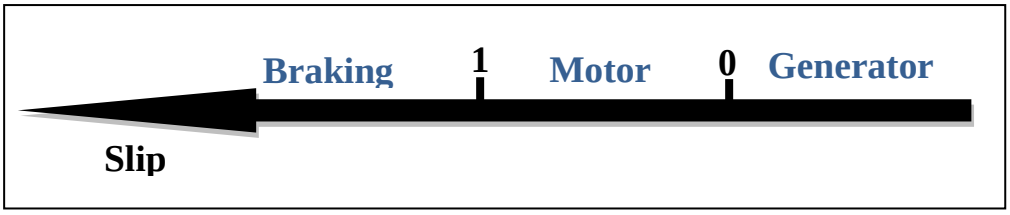

Figure I.1: Operational Modes Based on Slip

I.5.1 Key strengths of multi-phase machines:

Multiphase machines, particularly dual three-phase induction motors, offer several benefits over traditional three-phase systems:

- Enhanced Fault Tolerance: The increased number of phases allows for continued operation even if one or more phases fail, improving system reliability.
- Reduced Torque Ripple: The distribution of phases leads to smoother torque production, minimizing mechanical vibrations and enhancing performance.
- Lower Harmonic Distortion: Multiphase systems exhibit reduced harmonic content, leading to improved power quality and reduced electromagnetic interference.
- Improved Efficiency: The design of multiphase machines can lead to better utilization of materials and reduced losses, contributing to overall energy efficiency.
- Increased Power Density: By utilizing multiple phases, these machines can deliver higher power outputs without a proportional increase in size.

These advantages make multiphase machines particularly suitable for applications requiring high reliability and performance [7].

I.5.2 Technical challenges of multi-phase machines:

Despite their benefits, multiphase machines have certain drawbacks:

- Increased Complexity: The additional phases introduce more complex control and protection schemes, necessitating advanced algorithms and hardware.
- Higher Cost: The need for more components, such as additional power electronics and sensors, can lead to increased initial investment and maintenance costs.
- Design Challenges: The electromagnetic design becomes more intricate, requiring careful consideration to avoid issues like unbalanced loading and to ensure optimal performance.

These challenges must be addressed to fully realize the potential of multiphase machines in various applications [7].

In our work we are interested in the dual three-phase induction machine

I.6 Dual three-phase induction machine models:

The control of multiphase machines typically extends the fundamental principles used in controlling three-phase machines. Similar to three-phase systems, effective control relies on selecting an appropriate mathematical model for the machine. For dual three-phase induction machines, two main modeling approaches are widely employed in control system design: the **double-dq model** and the **VSD model**.

In the double-dq method, each of the two three-phase winding sets undergoes a separate Clarke transformation, resulting in two sets of stationary-frame α-β currents (iα1–iβ1 and iα2–iβ2), using stator currents as a reference. These are then converted to the rotating reference frame through Park transformation, yielding two d-q current pairs (id1 iq1 and id2 iq2). With the d-axis aligned to the rotor flux, flux control is achieved by regulating id1 and id2, while torque control is handled through iq1 and iq2. This concept mirrors the rotor flux-oriented control (RFOC) method used in three-phase systems but requires two sets of d-q controllers instead of one.

This model has been successfully implemented in literature, and extended to nine-phase machines for specific applications like ultra-high-speed elevators, using three sets of decoupling transformations and three d-q controller pairs. However, a notable limitation of this model is its reliance on multiple three-phase winding groups, making it less flexible for other multiphase configurations [8].

Alternatively, the **VSD model**, proposed in, serves as a powerful analytical framework for polyphase machine analysis and current control design. It decomposes an n-phase machine into n/2 orthogonal subspaces or ((n-1)/2 in the case of odd-phase machines), including one α-β subspace and several x-y subspaces, along with homopolar components. For machines with sinusoidal magnetomotive force (MMF) distribution, only the α-β components are involved in energy conversion, while x-y and zero-sequence components contribute to system losses. The VSD formulation makes the α-β equations of a polyphase machine identical to those of a three-phase machine, facilitating the direct application of conventional three-phase vector control strategies. However, the presence of non-energy-contributing components means that their associated currents must be controlled as well to enhance overall performance.

Compared to the double-dq approach, the VSD model offers broader applicability across various multiphase systems. By clearly separating torque- and flux-producing components (α-β) from loss-inducing ones (x-y and zero-sequence), it provides valuable insight for developing spatial vector pulse width modulation (SVPWM) techniques—something not easily achievable with the double-dq model.

While both models yield comparable dynamic performance in control applications, it has been observed that the VSD-based control requires less complex voltage decoupling terms than the double-dq approach. Despite being applicable to the same machine, the two models differ in terms of their parameter sets. If the mutual leakage inductance between the two winding sets is assumed negligible, a straightforward relationship can be established between both models. The stator resistance and leakage inductance remain identical, while the VSD model's mutual inductance, rotor leakage inductance, and rotor resistance are double those in the double-dq model [9].

Although the VSD model has clear analytical benefits, its variables lack direct physical association, making interpretation more challenging. Conversely, the double-dq model provides intuitive links: dq1 corresponds to the first (Star 1) winding group, and dq2 to the second (Star 2). Owing to this clarity and physical interpretability, the **double-dq model** is chosen for use in this work [10].

I.7 State of the art in the control of dual three-phase induction machines:

Various control strategies have been investigated for regulating induction machines. These techniques, designed to replace traditional vector control, include methods such as Direct Torque Control (DTC) and Sliding Mode Control (SMC), which are known for their strong robustness in handling parameter variations. The following control methods are commonly applied to asynchronous machines:

- ✓ In [11], Direct Torque Control of a Double Star Asynchronous Machine without Mechanical Sensor Using Artificial Intelligence Techniques by Mohammed Hechelef, 2017.

  This work improves direct torque control (DTC) using neural networks and fuzzy logic, with rotor speed estimation by classical and neural adaptive models.
- ✓ In [12], Nonlinear Control of a Double Star Asynchronous Machine "MASDE" by Mohamed Said Bilal & Salah Eddine Berrabah, 2019. This work studies vector control (DFOC) with a PI regulator, which is later replaced by a sliding mode controller to

enhance robustness against parameter variations.

- ✓ In [13], Field Oriented Control of Induction Motors Based on DSP Controller by BOUKHTACHE Seyfeddine and MESSINI Merouane, 2016 – The research Implements full FOC algorithm using space-vector PWM and DSP
- ✓ In [14], Fault-Tolerant Control of the Double Star Asynchronous Machine by Noureddine Layadi, 2020. This thesis develops fault-tolerant control (both passive and active) based on Backstepping and artificial intelligence techniques, such as type-2 fuzzy logic and neural networks, with a comparative performance analysis.
- ✓ In [15], Estimation of Speed and Stator and Rotor Resistances for Field-Oriented Control of an Asynchronous Machine for DIEDHIOU Tidjini 2018. The thesis enhances FOC accuracy by estimating key parameters, improving asynchronous machine control performance.
- ✓ In [16], Sliding Mode Control of the Double Star Asynchronous Machine by SOUSSA CHEMS EDDINE and WALID ABADI and HOUCINE GABOUSSA and ABDELDGALIL HECHIFA 2022. This thesis adopts PI regulators in vector control by flux orientation for the sliding mode control of a double star asynchronous machine.
- ✓ In [17], High Performance Control of a Six-Phase Induction Machine Using Multilevel converters by Selatna Hamza , Selatna Hichem and Hechifa Abdelhak 2023. This work focuses on improving the control performance of the six-phase induction machine (6PH-IM), particularly in high-power industrial applications such as rail traction and ship propulsion, by employing multilevel inverters.

I.8 Application of the dual three-phase induction machines:

Dual three-phase induction machines have demonstrated significant potential across various industrial sectors, especially where high power, reliability, and fault tolerance are critical. Their ability to continue operating under fault conditions and the advantages offered by power segmentation make them suitable for numerous demanding applications. The main areas of application include:

- **Railway Traction Systems**

Dual three-phase induction machines are widely used in electric locomotives and metro systems due to their ability to handle high torque demands and their robust fault-tolerant behavior. In the event of a partial system failure, the machine can continue to operate, ensuring the safety and continuity of transport operations. [18]

- **Naval and Marine Propulsion**

The marine industry benefits from dual three-phase induction machines due to their high efficiency and reliability in harsh environments. Ships and submarines often use six-phase motors to achieve propulsion because of their high torque capabilities and capacity to maintain operation under fault conditions, which is crucial for avoiding operational downtime at sea. [19]

- **Wind Energy Conversion Systems**

In wind turbine applications, dual three-phase induction machines offer improved power density and better fault tolerance compared to conventional machines. Their ability to operate even with a failed phase makes them a reliable choice for remote or offshore wind farms where maintenance access is limited. [20]

- **Aerospace Applications**

The aerospace sector requires lightweight, high-efficiency, and fault-tolerant machines. Dual three-phase induction machines, due to their segmented power structure, offer redundancy and safety in critical systems like electric propulsion units and onboard auxiliary systems. [21]

- **Electric and Hybrid Vehicles (EV/HEV)**

In electric and hybrid vehicles, dual three-phase induction machines are used to achieve higher efficiency and smoother torque delivery. Their ability to reduce phase current and share the load across multiple phases improves thermal management and extends the lifespan of components, especially in high-performance vehicles. [22]

- **Oil and Gas Industry**

For applications such as drilling, pumping, and offshore platforms, where reliability is paramount, dual three-phase induction machines are advantageous due to their robustness, fault tolerance, and the ability to operate under variable speed conditions. [23]

- **Industrial Automation and Robotics**

In automated systems and robotic platforms that require precision and reliability, dual three-phase induction machines provide enhanced control resolution and reduced torque ripple, improving overall system performance. [4]

These applications demonstrate the versatility and growing importance of dual three-phase induction machines in modern electrical engineering, especially in high-demand and mission-critical environments.

I.9 Conclusion:

This chapter presents a review of the evolution of electric machines, including their structure and principles of operation. It covers existing configurations, modeling approaches, and the main control strategies developed for multiphase systems. The benefits and limitations of each method are discussed based on previous research conducted by various authors in the field of multiphase machine control.

The following chapter will focus on the modeling and vector control of the dual three phase induction machines supplied by two voltage-source inverters.

CHAPTER II

Dual three-phase induction machines: Study and Modeling

II.1 introduction:

The modeling of any system is necessary for the application of a particular control method. In this chapter, we will focus on the modeling of the different parts of the studied system, which consists of the dual three-phase induction machines, the converters, and the DC bus. In fact, the modeling of the electrical machine involves very complex equations; the distribution of the windings and the specific geometry of the dual three-phase induction machines make its model difficult to implement. However, the adoption of certain simplifying assumptions allows us to overcome this complexity.

In this chapter, the modeling of the dual three-phase induction machines fed by two power converters is presented. In this study, an angular offset of the dual three-phase induction machines, $\alpha = 30°$ (angle between adjacent phases), is considered. Finally, simulation results will be presented and discussed.

II.2 Dual three-phase induction machines description:

The dual three-phase induction machines is composed of a stator equipped with two identical three-phase windings that are spatially shifted by an electrical angle of $\alpha = 30°$, along with a squirrel-cage rotor. Figure II.1 illustrates the schematic arrangement of the dual three-phase induction machine windings. The angles θr and $(\theta r - \alpha)$ represent the rotor position (phase ar) relative to the first stator winding set (phase as1) and the second stator winding set (phase as2), respectively. Electrical quantities associated with the two sets of stator windings (star 1 and star 2) are identified by the subscripts 1 and 2, accordingly [24].

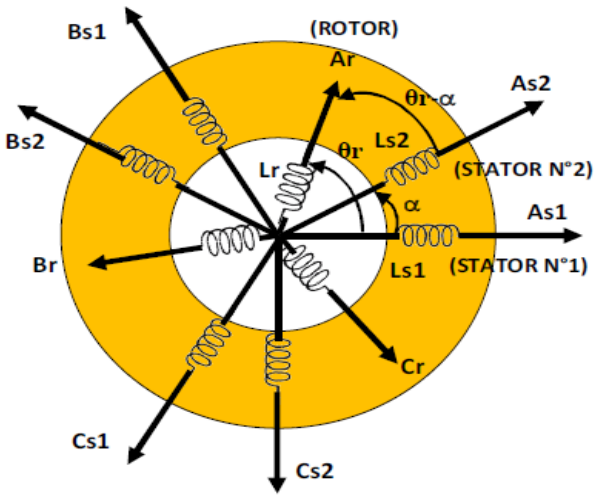

Figure II.1: Schematic diagram of the dual three-phase induction machine windings.

II.3 Simplifying assumptions:

Due to the complexity of the dual three-phase induction machine, particularly the distribution of its windings and its specific geometric structure, a detailed analysis considering its exact physical configuration is extremely difficult. As previously mentioned, it becomes essential to adopt a set of simplifying assumptions to facilitate the modeling process [25].

The following assumptions are considered in this study:

- The magnetic circuit operates in the linear region (unsaturated), allowing flux linkages to be expressed as linear functions of the currents.
- Core losses, including hysteresis and eddy current losses, are neglected. It is assumed that the magnetomotive forces (MMFs) produced by each phase of both stator winding sets are sinusoidally distributed.
- The effect of temperature variations on the stator and rotor resistances is considered negligible.
- The machine is assumed to have perfect symmetry, both electrically and magnetically.
- The air gap between the stator and rotor is uniform and constant.
- The skin effect in conductors is neglected.

II.4 Modeling of the dual three-phase induction machine:

II.4.1 Electrical equation:

The voltage expressions for the dual three-phase induction machine describe, for each winding, the sum of the resistive voltage drop and the voltage induced by the magnetic flux.
For star 1:

$$\begin{cases} U_{as1} = R_{s1} i_{as1} + \dfrac{d\varphi_{as1}}{dt} \\ U_{bs1} = R_{s1} i_{bs1} + \dfrac{d\varphi_{bs1}}{dt} \\ U_{cs1} = R_{s1} i_{cs1} + \dfrac{d\varphi_{cs1}}{dt} \end{cases} \quad \text{(II.1)}$$

For star 2:

$$\begin{cases} U_{as2} = R_{s2} i_{as2} + \dfrac{d\varphi_{as2}}{dt} \\ U_{bs2} = R_{s2} i_{bs2} + \dfrac{d\varphi_{bs2}}{dt} \\ U_{cs2} = R_{s2} i_{cs2} + \dfrac{d\varphi_{cs2}}{dt} \end{cases} \quad \text{(II.2)}$$

For rotor:

$$\begin{cases} 0 = U_{ar} = R_r i_{ar} + \dfrac{d\varphi_{ar}}{dt} \\ 0 = U_{br} = R_r i_{br} + \dfrac{d\varphi_{br}}{dt} \\ 0 = U_{cr} = R_r i_{cr} + \dfrac{d\varphi_{cr}}{dt} \end{cases} \quad \text{(II.3)}$$

In matrix form, we have:

For star 1: $$[U_{s1}] = [R_{s1}][i_{s1}] + \frac{d}{dt}[\varphi_{s1}] \quad \text{(II.4)}$$

For star 2: $$[U_{s2}] = [R_{s2}][i_{s2}] + \frac{d}{dt}[\varphi_{s2}] \quad \text{(II.5)}$$

For rotor: $$[U_r] = [R_r][i_r] + \frac{d}{dt}[\varphi_r] \quad \text{(II.6)}$$

With :

$$[U_{s1}] = \begin{bmatrix} U_{as1} \\ U_{bs1} \\ U_{cs1} \end{bmatrix} ; [U_{s2}] = \begin{bmatrix} U_{as2} \\ U_{bs2} \\ U_{cs2} \end{bmatrix} ; [U_r] = \begin{bmatrix} U_{ar} \\ U_{br} \\ U_{cr} \end{bmatrix} \quad \text{(II.7)}$$

$[U_{s1}]$: Star 1 voltage matrix ;

$[U_{s2}]$: Star 2 voltage matrix;

$[U_r]$: Rotor Voltage Matrix.

With :

$$[i_{s1}] = \begin{bmatrix} i_{as1} \\ i_{bs1} \\ i_{cs1} \end{bmatrix} ; [i_{s2}] = \begin{bmatrix} i_{as2} \\ i_{bs2} \\ i_{cs2} \end{bmatrix} ; [i_r] = \begin{bmatrix} i_{ar} \\ i_{br} \\ i_{cr} \end{bmatrix} \quad \text{(II.8)}$$

$[i_{s1}]$:Current matrix of star 1;

$[i_{s2}]$: Current matrix of star 2;

$[i_r]$: Rotor current matrix.

With :

$$R_{as1} = R_{bs1} = R_{cs1} \; ; \; R_{as2} = R_{bs2} = R_{cs2} \text{ et } R_{ar} = R_{br} = R_{cr} \tag{II.9}$$

$$[R_{s1}] = \begin{bmatrix} R_{as1} & 0 & 0 \\ 0 & R_{bs1} & 0 \\ 0 & 0 & R_{cs1} \end{bmatrix} ; \quad [R_{s2}] = \begin{bmatrix} R_{as2} & 0 & 0 \\ 0 & R_{bs2} & 0 \\ 0 & 0 & R_{cs2} \end{bmatrix} ; [R_r] = \begin{bmatrix} R_{ar} & 0 & 0 \\ 0 & R_{br} & 0 \\ 0 & 0 & R_{cr} \end{bmatrix} \tag{II.10}$$

$[R_{s1}]$:Resistance of a star phase 1;

$[R_{s2}]$: Resistance of a phase of star 2;

$[R_r]$: Resistance of a phase of the rotor.

$$[\varphi_{s1}] = \begin{bmatrix} \varphi_{as1} \\ \varphi_{bs1} \\ \varphi_{cs1} \end{bmatrix} ; [\varphi_{s2}] = \begin{bmatrix} \varphi_{as2} \\ \varphi_{bs2} \\ \varphi_{cs2} \end{bmatrix} ; [\varphi_r] = \begin{bmatrix} \varphi_{ar} \\ \varphi_{br} \\ \varphi_{cr} \end{bmatrix} \tag{II.11}$$

$[\varphi_{s1}]$: Flux matrix of star 1;

$[\varphi_{s2}]$: Flux matrix of star 2;

$[\varphi_r]$: Rotor flux matrix.

II.4.2 Magnetic equations:

The stator and rotor flux linkages, in terms of currents, self-inductances, and mutual inductances, are represented using the matrix expressions given by the following equations [26]:

$$[L(\theta)] = \begin{bmatrix} [L_{s1,s1}] & [M_{s1,s2}] & [M_{s1,r}] \\ [M_{s2,s1}] & [L_{s2,s2}] & [M_{s2,r}] \\ [M_{r,s1}] & [M_{r,s2}] & [L_{r,r}] \end{bmatrix} \tag{II.12}$$

$$\begin{bmatrix} [\varphi_{s1}] \\ [\varphi_{s2}] \\ [\varphi_r] \end{bmatrix} = [L(\theta)] \begin{bmatrix} [i_{s1}] \\ [i_{s2}] \\ [i_r] \end{bmatrix} \tag{II.13}$$

The sub-matrices of the inductance matrix are expressed as follows:

$$[L_{s1,s1}]=\begin{bmatrix} (L_{s1}+L_{ms}) & L_{ms}\cos\left(\frac{2\pi}{3}\right) & L_{ms}\cos\left(\frac{4\pi}{3}\right) \\ L_{ms}\cos\left(\frac{4\pi}{3}\right) & (L_{s1}+L_{ms}) & L_{ms}\cos\left(\frac{2\pi}{3}\right) \\ L_{ms}\cos\left(\frac{2\pi}{3}\right) & L_{ms}\cos\left(\frac{4\pi}{3}\right) & (L_{s1}+L_{ms}) \end{bmatrix} \quad \text{(II.14)}$$

$$[L_{s2,s2}]=\begin{bmatrix} (L_{s2}+L_{ms}) & L_{ms}\cos\left(\frac{2\pi}{3}\right) & L_{ms}\cos\left(\frac{4\pi}{3}\right) \\ L_{ms}\cos\left(\frac{4\pi}{3}\right) & (L_{s2}+L_{ms}) & L_{ms}\cos\left(\frac{2\pi}{3}\right) \\ L_{ms}\cos\left(\frac{2\pi}{3}\right) & L_{ms}\cos\left(\frac{4\pi}{3}\right) & (L_{s2}+L_{ms}) \end{bmatrix} \quad \text{(II.15)}$$

$$[L_{r,r}]=\begin{bmatrix} (L_{r}+L_{mr}) & L_{mr}\cos\left(\frac{2\pi}{3}\right) & L_{mr}\cos\left(\frac{4\pi}{3}\right) \\ L_{mr}\cos\left(\frac{4\pi}{3}\right) & (L_{r}+L_{mr}) & L_{mr}\cos\left(\frac{2\pi}{3}\right) \\ L_{mr}\cos\left(\frac{2\pi}{3}\right) & L_{mr}\cos\left(\frac{4\pi}{3}\right) & (L_{r}+L_{mr}) \end{bmatrix} \quad \text{(II.16)}$$

$$[M_{s1,s2}]=\begin{bmatrix} L_{ms}\cos(\alpha) & L_{ms}\cos\left(\alpha+\frac{2\pi}{3}\right) & L_{ms}\cos\left(\alpha+\frac{4\pi}{3}\right) \\ L_{ms}\cos\left(\alpha+\frac{4\pi}{3}\right) & L_{ms}\cos(\alpha) & L_{ms}\cos\left(\alpha+\frac{2\pi}{3}\right) \\ L_{ms}\cos\left(\alpha+\frac{2\pi}{3}\right) & L_{ms}\cos\left(\alpha+\frac{4\pi}{3}\right) & L_{ms}\cos(\alpha) \end{bmatrix} \quad \text{(II.17)}$$

$$[M_{s1,r}]=\begin{bmatrix} L_{sr}\cos(\theta_r) & L_{sr}\cos\left(\theta_r+\frac{2\pi}{3}\right) & L_{sr}\cos\left(\theta_r+\frac{4\pi}{3}\right) \\ L_{sr}\cos\left(\theta_r+\frac{4\pi}{3}\right) & L_{sr}\cos(\theta_r) & L_{sr}\cos\left(\theta_r+\frac{2\pi}{3}\right) \\ L_{sr}\cos\left(\theta_r+\frac{2\pi}{3}\right) & L_{sr}\cos\left(\theta_r+\frac{4\pi}{3}\right) & L_{sr}\cos(\theta_r) \end{bmatrix} \quad \text{(II.18)}$$

$$[M_{s2,r}]=\begin{bmatrix} L_{sr}\cos(\theta_r-\alpha) & L_{sr}\cos\left(\theta_r-\alpha+\frac{2\pi}{3}\right) & L_{sr}\cos\left(\theta_r-\alpha+\frac{4\pi}{3}\right) \\ L_{sr}\cos\left(\theta_r-\alpha+\frac{4\pi}{3}\right) & L_{sr}\cos(\theta_r-\alpha) & L_{sr}\cos\left(\theta_r-\alpha+\frac{2\pi}{3}\right) \\ L_{sr}\cos\left(\theta_r-\alpha+\frac{2\pi}{3}\right) & L_{sr}\cos\left(\theta_r-\alpha+\frac{4\pi}{3}\right) & L_{sr}\cos(\theta_r-\alpha) \end{bmatrix} \quad \text{(II.19)}$$

$$\left[M_{s2,s1}\right]=\left[M_{s1,s2}\right]^t \;;\; \left[M_{r,s1}\right]=\left[M_{s1,r}\right]^t \;;\left[M_{r,s2}\right]=\left[M_{s2,r}\right]^t \qquad \text{(II.20)}$$

$$L_{ms}=L_{mr}=L_{sr}=\frac{2}{3}L_m \qquad \text{(II.21)}$$

With :

L_{s1} :The self-inductance of the stator1;

L_{s2} : The self-inductance of the stator2;

L_r : The self-inductance of a phase of the rotor;

L_{ms} : The maximum value of the stator mutual inductance coefficients;

L_{mr} : The maximum value of the rotor mutual inductance coefficients;

L_{sr} : The maximum value of the mutual inductance coefficients between a star and the rotor.

II.4.3 Magnetic energy:

The magnetic energy stored in the rotor can calculate from the following expression [27]:

$$w_{mag}=\frac{1}{2}\left(\left[i_{s1}\right]^t\left[\varphi_{s1}\right]+\left[i_{s2}\right]^t\left[\varphi_{s2}\right]+\left[i_r\right]^t\left[\varphi_r\right]\right) \qquad \text{(II.22)}$$

II.4.4 Electromagnetic torque:

The electromagnetic torque is derived by differentiating the co-energy with respect to the magnetic angle [28].

$$C_{em}=\frac{d}{d\theta_{mag}}w_{mag}=p\frac{d}{d\theta_e}w_{mag} \qquad \text{(II.23)}$$

With :

p : pole pair number.

θ_{mag} : magnetic angle.

θ_e : electric angle

$$C_{em} = \frac{p}{2}\left([i_{s1}] \frac{d}{d\theta_r} [L_{s1,r}] [i_r]^t + [i_{s2}] \frac{d}{d\theta_r} [L_{s2,r}] [i_r]^t \right) \quad \text{(II.24)}$$

With :

θ_r : Rotor position relative to star 1 [rd].

II.4.5 Mechanical equation:

The fundamental equation of rotor rotation is described by the following two relations [27]:

$$J \frac{d\Omega}{dt} = C_{méc} = C_g - C_{em} - C_f \quad \text{(II.25)}$$

With :

$$\Omega = \frac{\omega_r}{p} \quad \text{(II.26)}$$

On the other hand :

$$\omega_r = \frac{d\theta_r}{dt} \quad \text{(II.27)}$$

II.5 Park transformation:

To simplify the complex mathematical model of the physical system, orthogonal transformations are employed. These transformations enable the conversion of the original phase variables into a more manageable form, often resulting in simpler and more insightful dynamic equations. One of the most widely used techniques for this purpose is Park's transformation.

Park's transformation converts the three-phase stator windings (labeled a, b, and c) into a two-axis equivalent system, represented by d and q axes. This transformation allows the system to be analyzed as two fictitious windings that produce the same magnetomotive force (MMF) as the original system.

The transformation removes the homopolar component, as it does not contribute to torque production. The homopolar axis is typically chosen to be orthogonal to the (d, q) plane and thus doesn't influence the electromagnetic behavior relevant to torque and flux control [29].

II.5.1 Park's matrix in general:

For star 1 is defined as follows:

$$[P(\theta_{s1})] = \sqrt{\frac{2}{3}} \begin{bmatrix} \cos(\theta) & \cos\left(\theta - \frac{2}{3}\right) & \cos\left(\theta + \frac{2}{3}\right) \\ -\sin(\theta) & -\sin\left(\theta - \frac{2}{3}\right) & -\sin\left(\theta + \frac{2}{3}\right) \\ \frac{1}{\sqrt{2}} & \frac{1}{\sqrt{2}} & \frac{1}{\sqrt{2}} \end{bmatrix} \quad \text{(II.28)}$$

$$[P(\theta_{s1})]^{-1} = \sqrt{\frac{2}{3}} \begin{bmatrix} \cos(\theta) & -\sin(\theta) & \frac{1}{\sqrt{2}} \\ \cos\left(\theta - \frac{2}{3}\right) & -\sin\left(\theta - \frac{2}{3}\right) & \frac{1}{\sqrt{2}} \\ \cos\left(\theta + \frac{2}{3}\right) & -\sin\left(\theta + \frac{2}{3}\right) & \frac{1}{\sqrt{2}} \end{bmatrix} \quad \text{(II.29)}$$

• For star 2 and the rotor, we replace in (II.28) et (II.29) θ by $(\theta - \alpha)$ and then by $(\theta_{gl} = \theta - \theta_r)$ respectively.

II.5.2 Choice of reference frame:

Three types of frames of reference are interesting in practice, the choice of the frame of reference made according to the problem to be studied.

a) Reference frame linked to the stator ($\omega coor$=0).

$$\frac{d\theta_s}{dt} = 0 \quad \text{(II.30)}$$

$$\theta_s = \theta_r + \theta \quad \text{(II.31)}$$

$$\frac{d\theta_s}{dt} = 0 = \frac{d\theta_r}{dt} + \frac{d\theta}{dt} \quad \text{(II.32)}$$

$$\frac{d\theta_r}{dt} = -\frac{d\theta}{dt} = -p\Omega \quad \text{(II.33)}$$

This reference frame is stationary with respect to the stator, used for the study of starting and braking of alternating current machines with connection of resistors.

b) Reference frame linked to the rotor ($\omega_{coor}= \omega_r$).

$$\frac{d\theta_r}{dt} = 0 \tag{II.34}$$

$$\frac{d\theta_s}{dt} = \frac{d\theta}{dt} = p\Omega \tag{II.35}$$

This reference frame is stationary with respect to the rotor, used for the study of transient regimes in asynchronous and synchronous machines.

c) Reference frame linked to the rotating field $\omega_s = \omega_e$ et $\omega_r = \omega_e - \omega$

$$\frac{d\theta}{dt} = \omega_s \tag{II.36}$$

$$\frac{d\theta}{dt} = \omega_s - p\Omega \tag{II.37}$$

The latter is used to realize the vector control due to the fact that the manipulated quantities become continuous [30].

In our work, we used this reference for the modeling of the dual three-phase induction machine. Because this frame of reference is generally used with the aim of being able to apply a command of speed, torque, etc. since the quantities in this frame of reference are continuous. This system of "d, q" axes is fixed with respect to the electromagnetic field created by the stator windings, hence $\omega_{coor} = \omega_s$

The general expression of the Park transformation is obtained by the projection of the three-phase quantities of the machine on two perpendicular axes d and q.

$$X_{dqo} = P(\theta_s) X_{abc} \tag{II.38}$$

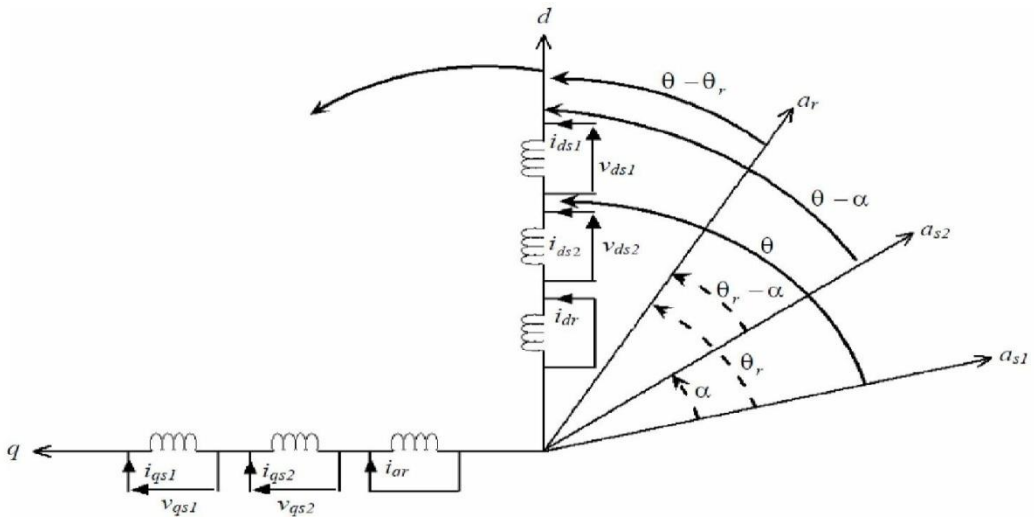

Figure II.2: The generalized model of dual three-phase induction machine along the axes.

II.5.3 Matrix equation with Park transformation:

The model of the dual three-phase induction machine in a two-phase reference frame linked to the rotating field is obtained by using the standardized Park transformations, which allow for the conservation of power. By applying these transformations to the voltages as well as the stator fluxes [31], with the null homopolar component, we obtain the following system of equations:

$$\begin{cases} U_{ds1} = R_{s1} i_{ds1} + \dfrac{d}{dt}\varphi_{ds1} - \omega_s \varphi_{qs1} \\ U_{qs1} = R_{s1} i_{qs1} + \dfrac{d}{dt}\varphi_{qs1} + \omega_s \varphi_{ds1} \\ U_{ds2} = R_{s2} i_{ds2} + \dfrac{d}{dt}\varphi_{ds2} - \omega_s \varphi_{qs2} \\ U_{qs2} = R_{s2} i_{qs2} + \dfrac{d}{dt}\varphi_{qs2} + \omega_s \varphi_{ds2} \\ U_{dr} = R_r i_{dr} + \dfrac{d}{dt}\varphi_{dr} - \omega_{gl} \varphi_{qr} \\ U_{qr} = R_r i_{qr} + \dfrac{d}{dt}\varphi_{qr} + \omega_{gl} \varphi_{dr} \end{cases} \qquad \text{(II.39)}$$

Or :

$$\omega_{gl} = \omega_s - \omega_r \qquad \text{(II.40)}$$

The components of the stator and rotor fluxes are expressed as follows:

$$\begin{cases} \phi_{ds1} = L_{s1} i_{ds1} + L_m \left(i_{ds1} + i_{ds2} + i_{dr} \right) \\ \phi_{qs1} = L_{s1} i_{qs1} + L_m \left(i_{qs1} + i_{qs2} + i_{qr} \right) \\ \phi_{ds2} = L_{s2} i_{ds2} + L_m \left(i_{ds1} + i_{ds2} + i_{dr} \right) \\ \phi_{qs2} = L_{s2} i_{qs2} + L_m \left(i_{qs1} + i_{qs2} + i_{qr} \right) \\ \phi_{dr} = L_r i_{dr} + L_m \left(i_{ds1} + i_{ds2} + i_{dr} \right) \\ \phi_{qr} = L_r i_{qr} + L_m \left(i_{qs1} + i_{qs2} + i_{qr} \right) \end{cases} \quad \text{(II.41)}$$

With :

$$\omega_s = \frac{d\theta}{dt} \quad \text{(II.42)}$$

$$\omega_r = \frac{d\theta_r}{dt} \quad \text{(II.43)}$$

$$p\Omega = \frac{d\theta}{dt} - \frac{d\theta_r}{dt} = \omega_s - \omega_r \quad \text{(II.44)}$$

With :

$L_{s1} + L_m$: Cyclic self-inductance of stator 1.

$L_{s2} + L_m$: Cyclic self-inductance of stator 2.

$L_r + L_m$: Rotor cyclic self-inductance.

$L_m = \frac{3}{2} L_{ms} = \frac{3}{2} L_{mr} = \frac{3}{2} L_{sr}$: Cyclic mutual inductance between star 1 and 2 and the rotor.

- Conversion into State-Space Form:

Putting the system in the form of a state, we find:

$$\left[\dot{I} \right] = [L]^{-1} \left([B][U] - \omega_{gl} [C][I] - [D][I] \right) \quad \text{(II.45)}$$

Or :

$$[B] = diag[1 \quad 1 \quad 1 \quad 1 \quad 0 \quad 0] \quad \text{(II.46)}$$

Command vector:

$$[U] = \left[U_{ds1}, U_{qs1}, U_{ds2}, U_{qs2}, U_{dr}, U_{qr} \right]^t \quad \text{(II.47)}$$

State vector :

$$[I]=\left[i_{ds1},i_{qs1},i_{ds2},i_{qs2},i_{dr},i_{qr}\right]^t \tag{II.48}$$

$$\left[\dot{I}\right]=\frac{d}{dt}[I] \tag{II.49}$$

$$[L]=\begin{bmatrix}(L_{s1}+L_m) & 0 & L_m & 0 & L_m & 0\\ 0 & (L_{s2}+L_m) & 0 & L_m & 0 & L_m\\ L_m & 0 & (L_{s2}+L_m) & 0 & L_m & 0\\ 0 & L_m & 0 & (L_{s2}+L_m) & 0 & L_m\\ L_m & 0 & L_m & 0 & (L_r+L_m) & 0\\ 0 & L_m & 0 & L_m & 0 & (L_r+L_m)\end{bmatrix} \tag{II.50}$$

$$[C]=\begin{bmatrix}0 & 0 & 0 & 0 & 0 & 0\\ 0 & 0 & 0 & 0 & 0 & 0\\ 0 & 0 & 0 & 0 & 0 & 0\\ 0 & 0 & 0 & 0 & 0 & 0\\ 0 & -L_m & 0 & -L_m & 0 & -(L_r+L_m)\\ L_m & 0 & L_m & 0 & (L_r+L_m) & 0\end{bmatrix} \tag{II.51}$$

$$[D]=\begin{bmatrix}R_{s1} & -\omega_s(L_{s1}+L_m) & 0 & -\omega_s L_m & 0 & -\omega_s L_m\\ \omega_s(L_{s1}+L_m) & R_{s1} & \omega_s L_m & 0 & \omega_s L_m & 0\\ 0 & -\omega_s L_m & R_{s2} & -\omega_s(L_{s2}+L_m) & 0 & -\omega_s L_m\\ \omega_s L_m & 0 & -\omega_s(L_{s2}+L_m) & R_{s2} & \omega_s L_m & 0\\ 0 & 0 & 0 & 0 & R_r & 0\\ 0 & 0 & 0 & 0 & 0 & R_r\end{bmatrix} \tag{II.52}$$

II.5.4 Power and electromagnetic torque:

The power of the dual three-phase induction machine in the system of axes (d, q), while neglecting the homopolar components is expressed by:

$$P_a=V_{ds1}i_{ds1}+V_{qs1}i_{qs1}+V_{ds2}i_{ds2}+V_{qs2}i_{qs2} \tag{II.53}$$

By replacing the voltages $(V_{ds1},V_{qs1},V_{ds2},V_{ds2})$ by their expressions in the equation we find:

$$P_a=\underbrace{\left[R_{s1}i_{ds1}^2+R_{s1}i_{qs1}^2+R_{s2}i_{ds2}^2+R_{s2}i_{qs2}^2\right]}_{Terme\ 1}+\underbrace{\left(\frac{d\varphi_{ds1}}{dt}i_{ds1}+\frac{d\varphi_{qs1}}{dt}i_{qs1}+\frac{d\varphi_{ds2}}{dt}i_{ds2}+\frac{d\varphi_{qs2}}{dt}i_{qs2}\right)}_{Terme\ 2}$$
$$+\underbrace{\omega_s\left(\varphi_{ds1}i_{qs1}-\varphi_{qs1}i_{ds1}+\varphi_{ds2}i_{qs2}-\varphi_{qs2}i_{ds2}\right)}_{Terme\ 3} \tag{II.54}$$

This expression consists of three components: the first represents the power losses due to the Joule effect, the second corresponds to the variation in electromagnetic energy (energy storage), and the third denotes the electromagnetic power supplied (Pem).

By comparing the general expression of electromagnetic power with the third term of the supplied power

$$P_{em} = \omega_s \left(\varphi_{ds1} i_{qs1} - \varphi_{qs1} i_{ds1} + \varphi_{ds2} i_{qs2} - \varphi_{qs2} i_{ds2} \right) \tag{II.55}$$

We find:

$$C_{em} = p\left(\varphi_{ds1} i_{qs1} - \varphi_{qs1} i_{ds1} + \varphi_{ds2} i_{qs2} - \varphi_{qs2} i_{ds2} \right) \tag{II.56}$$

$$C_{em} = \frac{P_{em}}{\Omega_s} = p \frac{P_{em}}{\omega_s} \tag{II.57}$$

Other expressions of the electromagnetic torque are possible. By replacing the expressions(II.40) in (II.56), we get [32]:

$$C_{em} = pL_m \left\{ \left(i_{qs1} + i_{qs2} \right) i_{dr} - \left(i_{ds1} + i_{ds2} \right) i_{qr} \right\} \tag{II.58}$$

From the rotor flux equations (φ_{dr} et φ_{qr}) expressed by (III.40), we get

$$i_{dr} = \frac{1}{L_m + L_r} \left[\varphi_{dr} - L_m \left(i_{ds1} + i_{ds2} \right) \right] \tag{II.59}$$

$$i_{qr} = \frac{1}{L_m + L_r} \left[\varphi_{qr} - L_m \left(i_{qs1} + i_{qs2} \right) \right] \tag{II.60}$$

By replacing (III.59) and (III.60) in the equation (III.58), we will have the relation of the electromagnetic torque in the Park frame (d, q) as follows:

$$C_{em} = p \frac{L_m}{L_m + L_r} \left\{ \left(i_{qs1} + i_{qs2} \right) \varphi_{dr} - \left(i_{ds1} + i_{ds2} \right) \varphi_{qr} \right\} \tag{II.61}$$

II.6 Dual three-phase induction machine simulation powered by sinusoidal voltages:

The simulation involves implementing the electromechanical model of the dual three-phase induction machine using the MATLAB/Simulink environment.

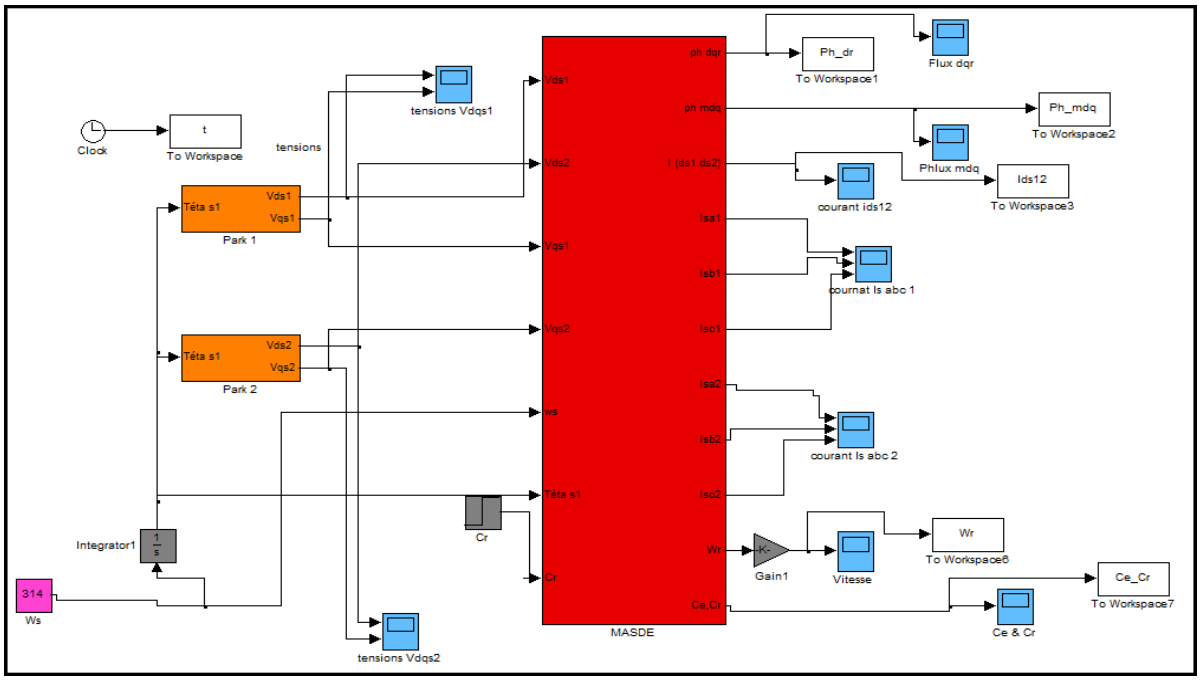

Figure II.3 : The simulation block diagram.

➢ Simulation Results:

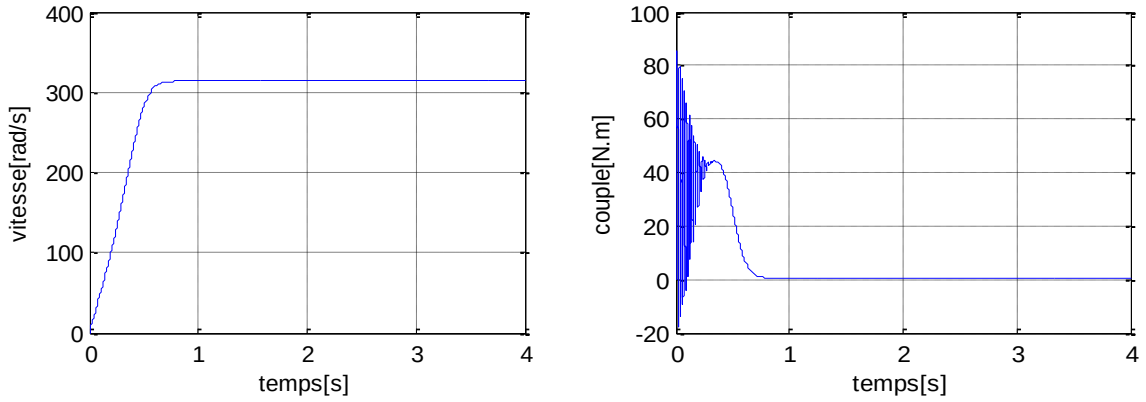

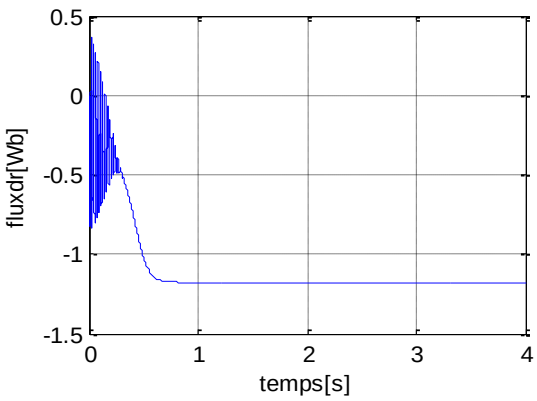
fluxdr[Wb]
temps[s]

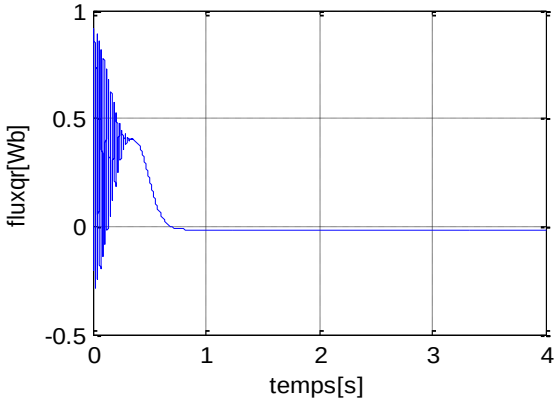
fluxqr[Wb]
temps[s]

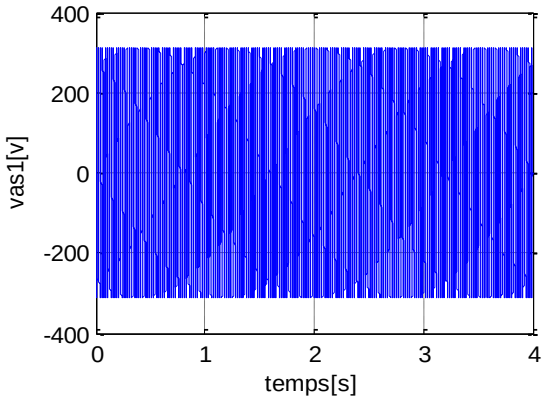
vas1[v]
temps[s]

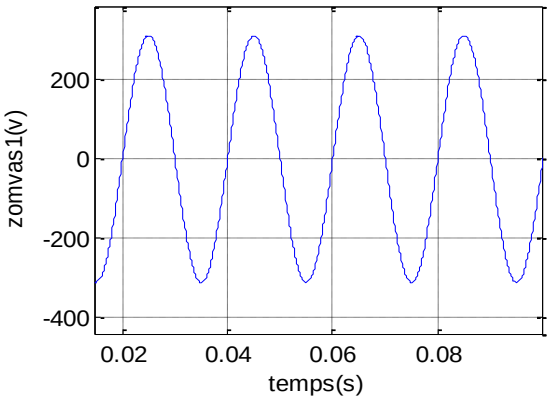
zomvas1(v)
temps(s)

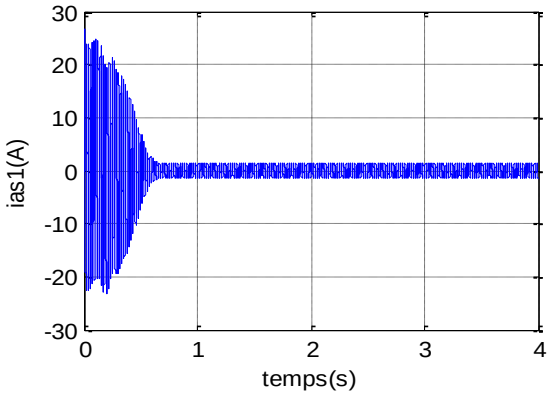
ias1(A)
temps(s)

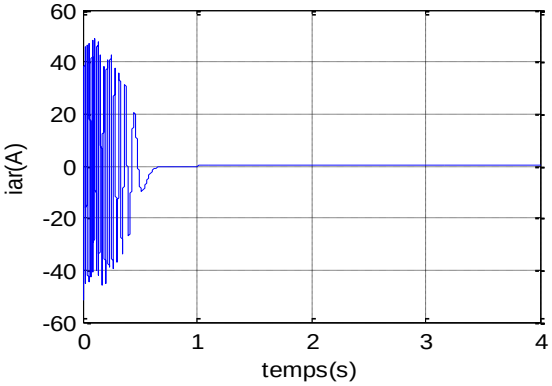
iar(A)
temps(s)

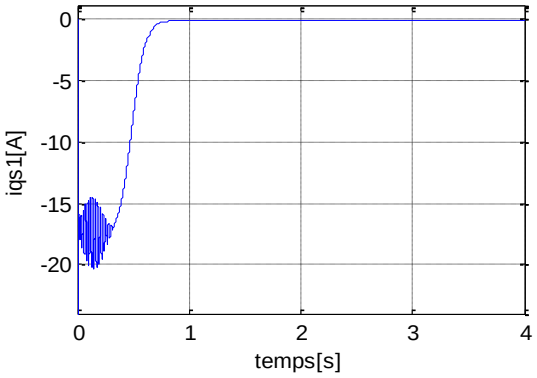
iqs1[A]
temps[s]

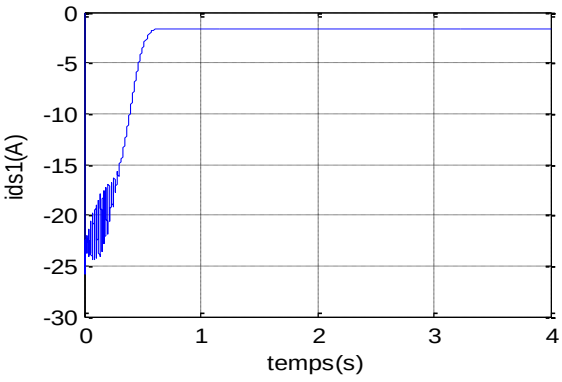
ids1(A)
temps(s)

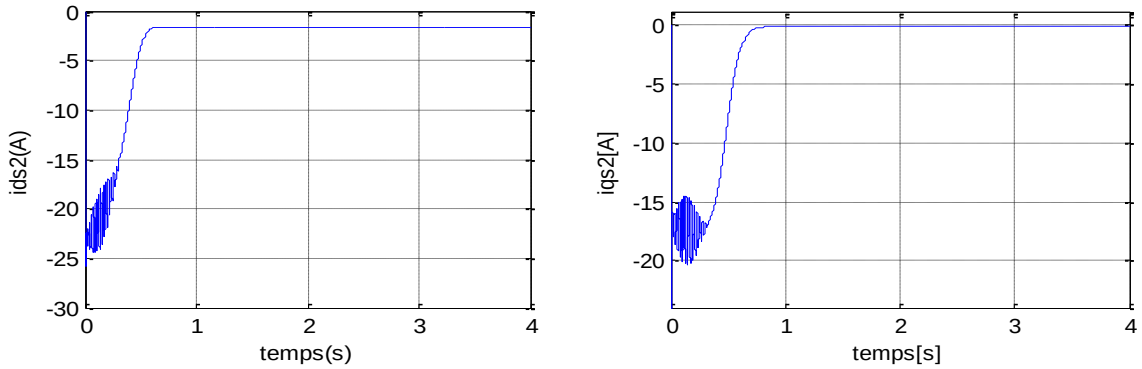

Figure II.4: Performance of the dual three-phase induction machine during no-load start-up

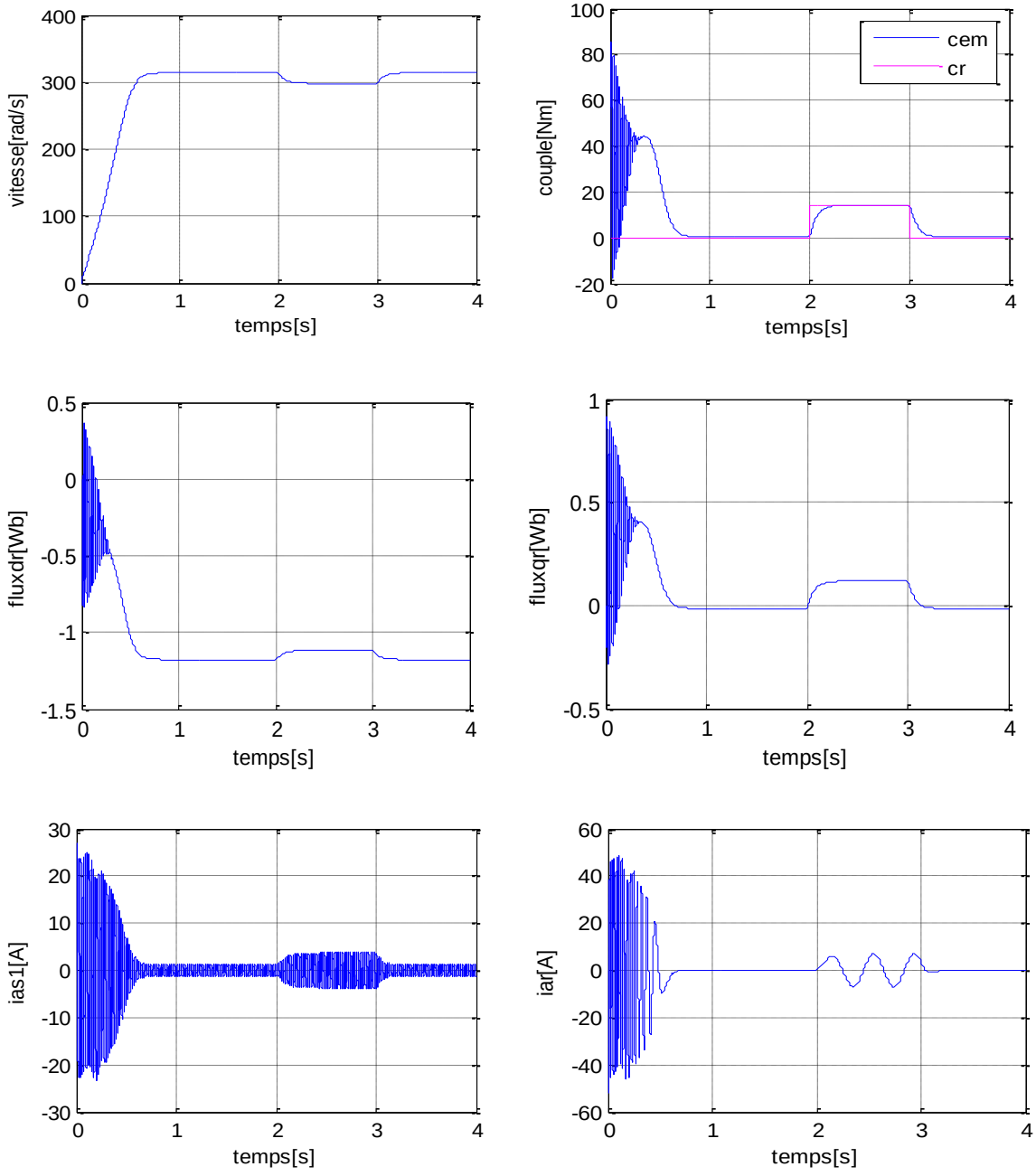

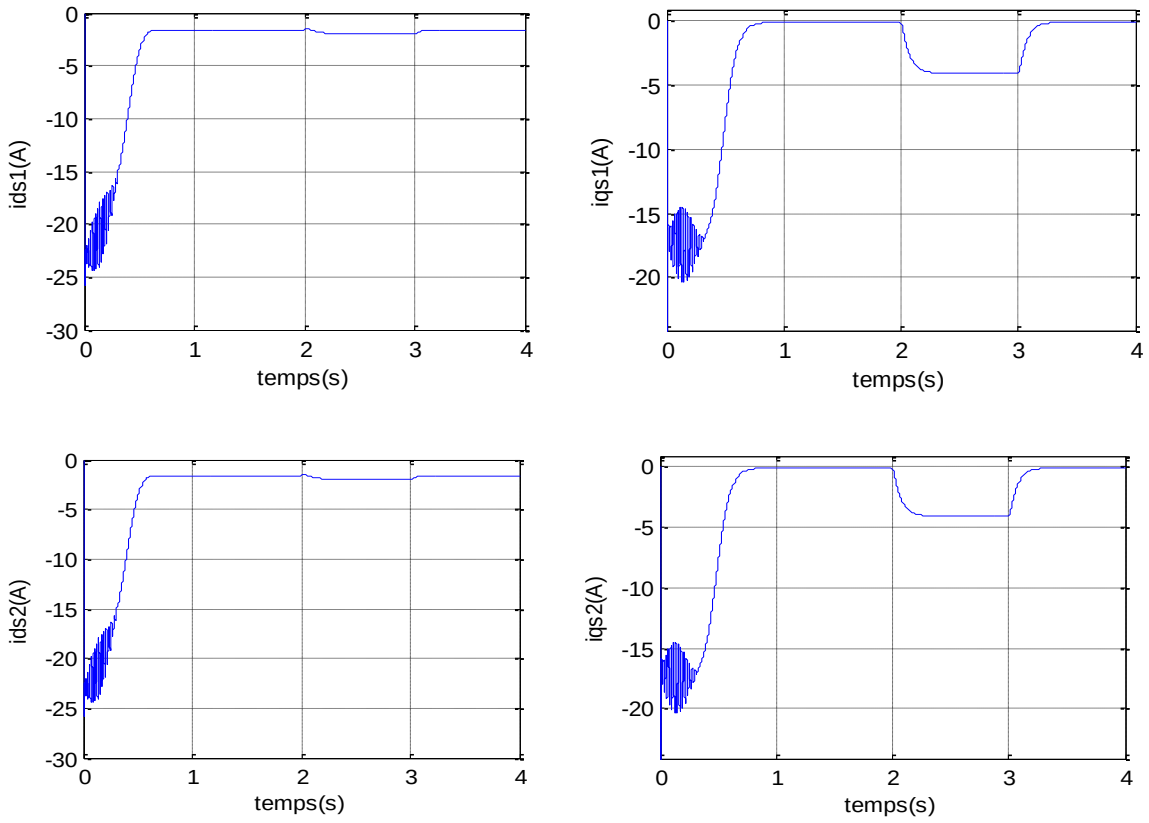

Figure II.5: Performance of dual three-phase induction machine with a load torque application of T = 14 N·m between 2s and 3s

]

We carried out a simulation of the operation of the dual three-phase induction machine, powered directly by a standard electrical network (220/380V, 50Hz), under both no-load and loaded conditions.

The simulation results, illustrated in Figures II.4 and II.5, show the evolution of several key variables of the induction machine. These include the rotational speed (ωr), electromagnetic torque (Cem), stator phase currents (i_{sa1}, i_{sa2}), the d- and q-axis currents (i_{sd1}, i_{sd2}, i_{sq1}, i_{sq2}), and rotor fluxes (flux rd, flux rq).

During startup and the transient phase, the speed increases almost linearly, reaching 313.8 rad/s at approximately t ≈ 0.8s (marking the beginning of steady-state operation).

Initially, the electromagnetic torque peaks at 85.4 N·m, then exhibits oscillations that diminish after 0.4s, eventually settling at 42.4 N·m before decreasing linearly and stabilizing at a minimal value of 0.314 N·m, due to friction.

The stator currents (for both stars 1 and 2) show high inrush peaks, reaching around four times the rated current. These peaks fade after a few cycles, giving way to steady sine waveforms of constant amplitude.

The direct and quadrature axis stator currents follow a pattern similar to that of the rotor speed, although slight oscillations are observed in the early 0.3s of the transient.

Rotor flux evolution closely mirrors that of the electromagnetic torque.

When a load torque of Cr = 14 N·m is applied between t = 2s and 3s (under motor operating conditions), the speed and d-q axis currents decrease and stabilize at wr = 298 rad/s, $i_{ds1} = i_{ds2} = -1.97$ A, and $i_{qs1} = i_{qs2} = -4.13$ A, respectively.

Conversely, increases are observed in electromagnetic torque, stator currents (stars 1 and 2), and rotor fluxes in the d-q reference frame, settling at Cem = 14.33 N·m (slightly above the applied torque), $i_{as1} = i_{as2} = 3.74$ A, flux dr = −1.11 Wb, and flux qr = 0.11 Wb.

In motor operation, the machine slip is slightly higher compared to the no-load case. The supply voltage Vas1 and stator current ias1 remain nearly in phase and have the same sign. Despite a slight lag of current behind voltage—due to the machine's inductive nature—their alignment in sign indicates that power flow is in the motoring direction (positive).

II.7 Conclusion:

In this chapter, we examined the modeling of the dual three-phase induction machine operating in motor mode. This modeling process enabled the development of a mathematical representation of the machine, with its complexity reduced through several simplifying assumptions. To facilitate simulation using MATLAB/Simulink, Park's transformation was applied to the system equations. The resulting simulations were then analyzed and interpreted.

The application of a load led to variations in speed and highlighted the strong coupling between the d and q axes, which makes independent control of each axis challenging. To address this issue, the following chapter introduces the vector control technique, based on flux orientation, which enables decoupling of the system and allows for independent control of each axis.

CHAPTER III

Field Oriented Control of Dual Three-Phase Induction Machine Based on PI Controllers

III.1 Introduction:

The concept of vector control was proposed by Blaschke in 1972, but its real-world application only became feasible with the emergence of advanced microelectronic technologies. This is due to the method's dependence on precise mathematical operations such as Park transformations, trigonometric function evaluations, integrations, and control regulations tasks that were impractical with analog systems alone.

In this chapter, the rotor flux-oriented vector control strategy is applied to the dual three-phase induction machine. A brief theoretical overview is provided to revisit the principles and methodologies associated with vector control. Following this, the control approach is implemented on the dual three-phase induction machine. The chapter concludes with a detailed discussion of the machine's dynamic performance, supported by simulation results.

III.2 Machine supply modeling:

In variable frequency machines, a static power converter is employed to generate and regulate the frequency and amplitude of the stator voltages or, alternatively, the amplitude of the stator currents required for machine operation. As the output frequency directly influences the rotational speed of the induction machine, accurate control of this parameter is critical.

The converter system utilized in this study comprises three main stages: a three-phase diode bridge rectifier connected to the AC supply network, which converts the alternating voltage into a DC link; an LC low-pass filter, designed to attenuate voltage and current ripple within the DC link; and finally, two pulse-width modulation (PWM) inverters one for each stator winding of the dual three-phase induction machine. These inverters generate variable-frequency, variable-amplitude AC voltages, enabling independent and flexible control of the machine's magnetic fields. The complete power supply configuration is illustrated in Figure III.1.

The performance of the electrical drive system is strongly influenced by the machine characteristics, the control strategy, and the structure of the static converter. The main requirements expected from the drive include:

- A torque output with minimal ripple, controllable with a minimal set of state variables in both transient and steady-state conditions.

- A wide speed regulation range.
- Low electrical and mechanical time constants to ensure rapid system response.
- A balanced three-phase supply system with constant amplitude and frequency assumptions for analysis.

These design criteria aim to ensure high dynamic performance, efficiency, and reliability of the overall control system [33].

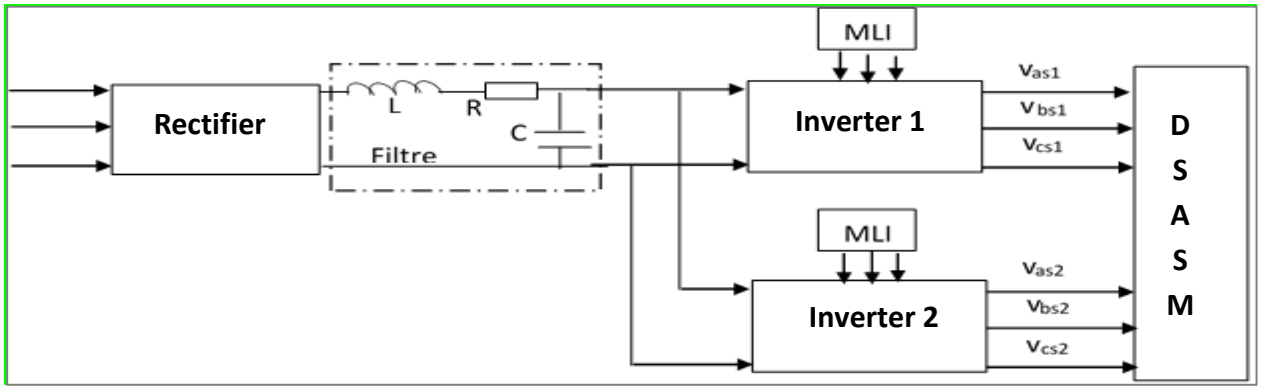

Figure III.1: Functional diagram of the dual three-phase induction machine fed by a dual-inverter power supply system.

III.2.1 Rectifier modeling:

In power electronics, diode and thyristor rectifiers are commonly employed to convert alternating current (AC) from single-phase or three-phase networks into direct current (DC). These rectifiers provide a continuous DC voltage of fixed or variable magnitude, suitable for direct application to loads or as an intermediate stage for other converters.

In our study focuses on a three-phase, uncontrolled, full-wave bridge rectifier utilizing diode components (Figure III.2). The rectifier is connected to a balanced three-phase AC supply, ensuring symmetrical voltage conditions.

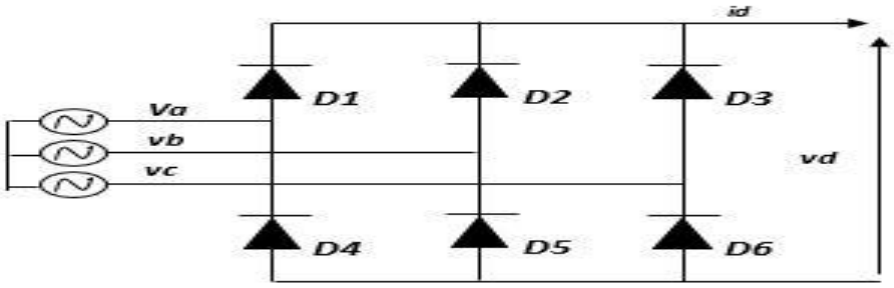

Figure III.2: Three-phase diode rectifier schematic.

The configuration comprises six diodes: three with common cathodes (D_1, D_2, D_3) facilitating current conduction, and three with common anodes (D_4, D_5, D_6) enabling current return. For analytical simplicity, diode voltage drops and losses are neglected. Under these assumptions, the rectifier operates with the following three-phase voltage inputs [34]:

$$U_a(t) = V_m \sin(wt) \quad \text{(III.1)}$$

$$U_b(t) = V_m \sin\left(wt - \frac{2\pi}{3}\right) \quad \text{(III.2)}$$

$$U_c(t) = V_m \sin\left(wt - \frac{4\pi}{3}\right) \quad \text{(III3.)}$$

The output voltage of the three-phase diode bridge rectifier can be expressed as:

$$U_{red}(t) = Max[U_a(t), U_b(t), U_c(t)] - Min[U_a(t), U_b(t), U_c(t)] \quad \text{(III.4)}$$

The average (DC) value of the rectified output voltage is calculated as:

$$U_{d\,moy} = \frac{3\sqrt{3}.\ V_m}{\pi} \quad \text{(III.5)}$$

The ripple factor, which quantifies the AC component in the rectified output, is determined by:

$$K\% = \frac{U_{d\,max} - U_{d\,min}}{2.\,U_{d\,moy}} = 7\% \quad \text{(III.6)}$$

Figure III.3 illustrates the temporal evolution of the three-phase input voltages (U_a, U_b, U_c) applied to the rectifier bridge, along with the resulting rectified output voltage U_d.

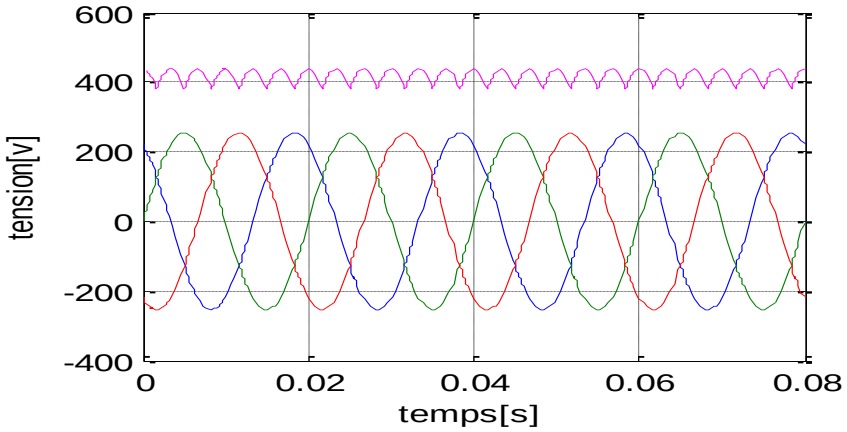

Figure III.3: Three-phase input and rectified output voltages.

The waveform produced at the rectifier output exhibits notable voltage ripple. To mitigate these fluctuations and achieve a smoother DC output, a filtering stage is required.

III.2.2 Filter modeling:

To attenuate voltage and current ripples at the output of the rectifier and ensure a stable DC link voltage for the inverters, an LC low-pass filter is employed between the rectifier bridge and the dual voltage inverters, as depicted in Figure III.4. This configuration effectively smooths the DC voltage and mitigates high-frequency harmonics introduced by the switching actions of the inverters.

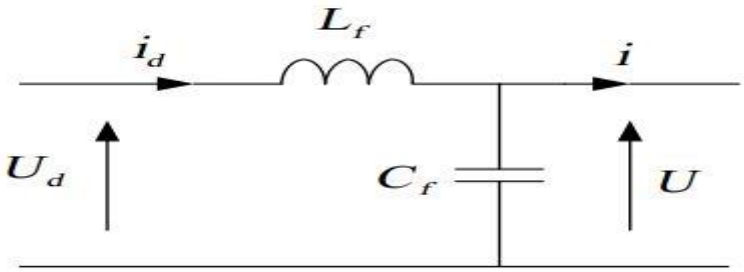

Figure III.4: LC Filter Configuration.

The capacitor C_f serves to maintain a substantially constant DC voltage U at the inverter input and absorbs the negative current returned by the load during transient conditions. The inductor L_f functions to reduce the ripple in the DC current i_d, thereby enhancing the quality of power supplied to the inverters [35].

The LC filter can be modeled by the following differential equations:

$$\begin{cases} U_d = L_f \frac{di_d}{dt} + U \\ \frac{dU}{dt} = \frac{1}{C_f}(i_d - \mathrm{I}) \end{cases} \quad \text{(III.7)}$$

The transfer function of the LC filter is given by:

$$F(s) = \frac{U(s)}{U_d(\mathrm{s})} = \frac{1}{L_f C_f s^2 + 1} \quad \text{(III.8)}$$

Which represents a second-order low-pass filter. The cutoff frequency f_c of the filter is determined by:

$$f_c = \frac{1}{\sqrt{L_f . C_f}} \quad \text{(III.9)}$$

In designing the filter, the values of L_f and C_f are selected to ensure that the cutoff frequency is significantly lower than the switching frequency of the inverters, thereby effectively attenuating high-frequency harmonics while maintaining system stability.

III.2.3 Two level inverters modeling:

Two-level voltage source inverters are widely utilized in variable-frequency drive applications due to their simplicity and effectiveness in converting DC power to AC power with controllable frequency and amplitude. In the context of dual three-phase induction machine, each stator winding set is typically fed by an independent three-phase two-level inverter, enabling precise control over the machine's electromagnetic fields.

Each inverter comprises three legs, with each leg consisting of two power switches (e.g., IGBT-diode pairs) arranged in a half-bridge configuration. The switches are operated in a complementary manner to prevent short circuits across the DC link. Assuming ideal switching devices, the output voltage of each phase leg can be modeled based on the switching states, facilitating the development of control strategies such as pulse-width modulation (PWM).

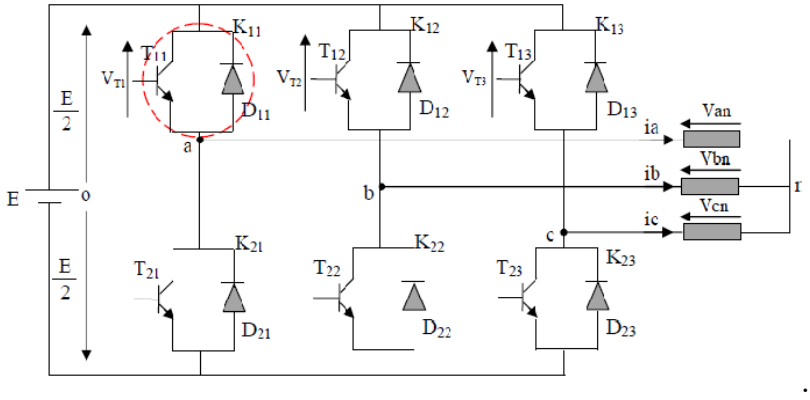

Figure III.5: Two-level three-phase inverter schematic.

The logical operation of each switch (Figure III.5), can be represented by a binary variable S_{ij} , where i=1,2,3 denotes the phase, and j=1,2 denotes the upper and lower switches, respectively [36]. The output voltage for each phase can then be expressed as:

$$V_{10} - V_a + V_b - V_{20} = 0 \qquad \text{(III.10)}$$

$$V_{10} - V_a + V_c - V_{30} = 0 \qquad \text{(III.11)}$$

Adding these equations, we get:

$$2V_{10} - 2V_a + V_b + V_c - V_{20} - V_{30} = 0 \qquad \text{(III.12)}$$

The single voltages form a balanced three-phase system such as:

$$V_a + V_b + V_c = 0 \tag{III.13}$$

In (III.12), we can replace by and we get

$$\begin{cases} V_a = \frac{1}{3}\left(2V_{10} - V_{20} - V_{30}\right) \\ V_b = \frac{1}{3}\left(-V_{10} + 2V_{20} - V_{30}\right) \\ V_c = \frac{1}{3}\left(-V_{10} - V_{20} + 2V_{30}\right) \end{cases} \tag{III.14}$$

The switching function S_{ij} takes the value of 1 when the corresponding switch is ON and 0 when OFF, and defined by the following logic connection function:

$$fi = \begin{cases} 1, & if\ switch\ i\ is\ closed \quad (Ki\ : Pass\ ,\ \bar{K}i: Block) \\ 0, & if\ switch\ i\ is\ Opened \quad (Ki: Block\ ,\ \bar{K}i: Pass) \end{cases} \tag{III. 15}$$

With:

$$f_i + \overline{f_i} = 1 \quad et \quad i = 1...3.$$

The equation in matrix form we have:

$$\begin{bmatrix} V_a \\ V_b \\ V_c \end{bmatrix} = \frac{E}{3}\begin{bmatrix} 2 & -1 & -1 \\ -1 & 2 & -1 \\ -1 & -1 & 2 \end{bmatrix}\begin{bmatrix} f_{11} \\ f_{21} \\ f_{31} \end{bmatrix} \tag{III.16}$$

III.3 Inverter sinusoidal PWM control strategy:

Pulse-width modulation (PWM) enables the conversion of a fixed-frequency, fixed-voltage DC source into AC voltages of variable amplitude and frequency with low harmonic distortion [37]. In this study, we employ the sinusoidal PWM (SPWM) technique. SPWM is generated by comparing a low-frequency sinusoidal reference waveform with a high-frequency triangular carrier signal. Switching events occur at the intersection points of the reference and carrier, and the inverter switching frequency is set by the carrier frequency. The sinusoidal reference voltages are expressed by:

For the first star:

$$\begin{cases} V_{refa1} = V_m \sin(2\pi ft) \\ V_{refb1} = V_m \sin(2\pi ft - \frac{2}{3}) \\ V_{refc1} = V_m \sin(2\pi ft + \frac{2}{3}) \end{cases} \quad \text{(III.17)}$$

For the second star; It suffices to replace in the system of equations , by and the index 1 by 2.

$$V_p(t) = \begin{cases} V_{pm}\left[4(t/T_p) - 1\right] & Si \quad 0 \le t \le T_p/2 \\ V_{pm}\left[-4(t/T_p) + 3\right] & Si \quad T_p/2 \le t \le T_p \end{cases} \quad \text{(III.18)}$$

This technique is characterized by the following two parameters:

- The modulation index m_{mod} equal to the ratio of the modulation frequency(f_p) on the reference frequency (f) ;
- The voltage adjustment coefficient r equal to the ratio of the amplitude of the reference voltage (V_m) at the peak value of the modulation wave (V_{pm})

The schematic diagram illustrating the connection of the dual three-phase induction machine with two voltage inverters utilizing sine-delta PWM control is shown in Figure III.6.

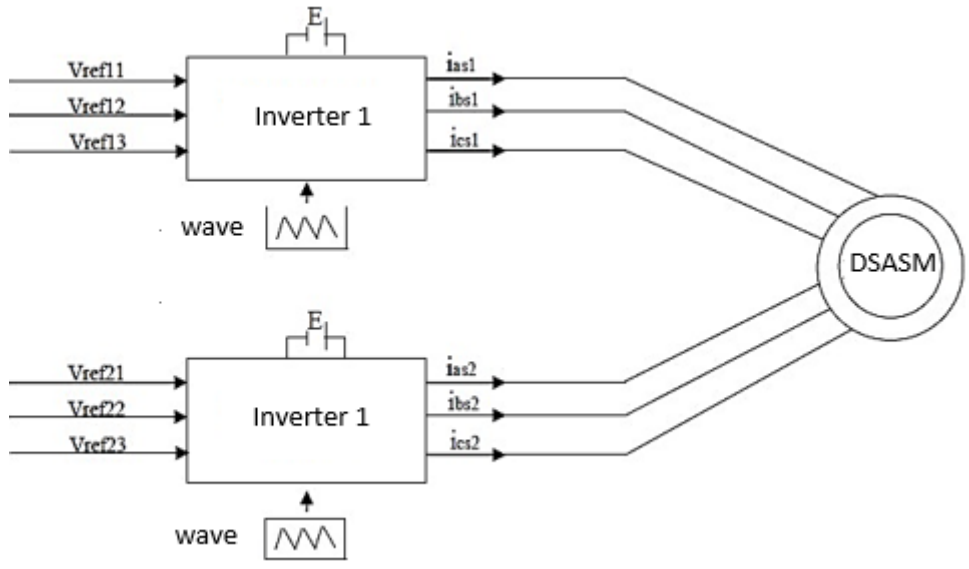

Figure III.6 : Integration of the dual three-phase induction machine static voltage inverters with PWM control

III.4 Vector Control:

III.4.1 The history of vector control:

The conceptual foundation of vector control can be traced back to the late 19th century with André Blondel's development of the two-reaction theory. This theory decomposed the armature magnetomotive force (MMF) of synchronous machines into two orthogonal components: the direct-axis (d-axis) and quadrature-axis (q-axis) components, facilitating a more precise analysis of machine behavior. However, due to technological limitations of that era, practical implementation in electric machine control was not feasible.

It wasn't until the early 1970s that advancements in control theory and power electronics enabled the practical application of these concepts. In particular, Felix Blaschke introduced the principle of field orientation, allowing for the independent control of torque and flux in AC machines, emulating the performance characteristics of separately excited DC machines [38].

III.4.2 The mathematical and control principles:

The fundamental concept behind vector control, also referred to as field-oriented control (FOC), is to align one component of the flux (stator, rotor, or air-gap) along a specific axis of a synchronously rotating reference frame at angular velocity ω_s. Although sometimes used interchangeably, “vector control” is a broader term, while “field-oriented control” is a specific implementation of vector control aimed at aligning the rotor flux. This technique enables the decoupling of torque and flux dynamics in an AC machine, thereby replicating the control simplicity of a separately excited DC machine, as illustrated in Figure III.7.

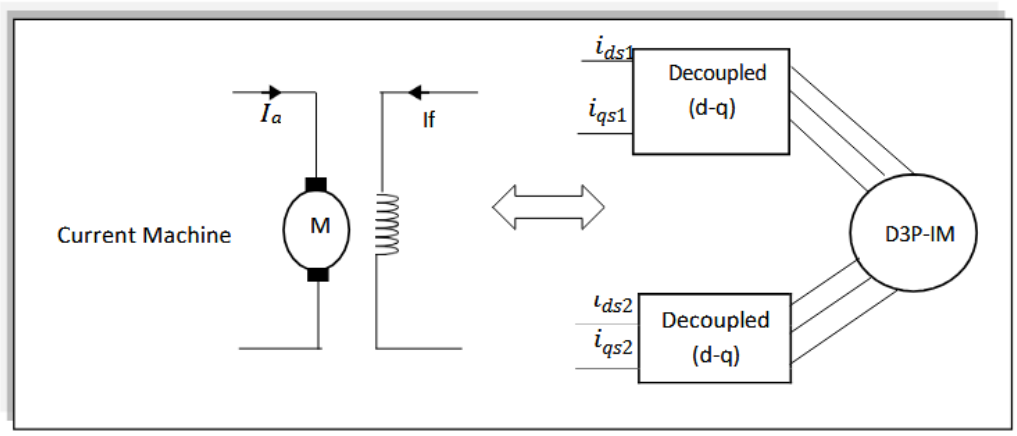

Figure III.7: The principle of vector control

In a DC machine, the torque is governed by the armature current , while the flux is independently controlled by the field current If. The electromagnetic torque C_{em} is expressed as:

$$C_{em} = K\Phi I_a = K' I_a \, I_f.$$

Where:

Φ : denotes the flux generated by the excitation current If.

Ia: Armature current.

K, K': Constants.

By emulating this decoupled behavior in dual three-phase induction machine using vector control, dynamic performance and precision in torque and flux control are significantly improved [38].

In the expression of the electromagnetic torque of dual three-phase induction machine, if we apply the orientation condition.

$$C_{em} = p\frac{L_m}{L_m+L_r}[(i_{qs1} + i_{qs2})\emptyset_{dr} - (i_{ds1} + i_{ds2})\emptyset_{qr}] \quad \text{(III.19)}$$

The equation then becomes:

$$C_{em} = p\frac{L_m}{L_m+L_r}\left[(i_{qs1} + i_{qs2})\emptyset_r\right] = \text{K''}\emptyset_r i_q \quad \text{(III.20)}$$

III.4.3 Flux orientation process:

In field-oriented control (FOC) of induction machines, the orientation of the flux vector is pivotal for decoupling torque and flux control. There are three primary flux orientation strategies:

- Rotor Flux Orientation: Aligns the d-axis of the rotating reference frame with the rotor flux vector, setting $\emptyset_{dr} = \emptyset_r \emptyset_{qr} = 0$
- Stator Flux Orientation: Aligns the d-axis with the stator flux vector, setting $\emptyset_{ds} = \emptyset_s \emptyset_{qs} = 0$
- Air-Gap Flux Orientation: Aligns the d-axis with the air-gap flux vector, setting $\emptyset_{dm} = \emptyset_m \, \emptyset_{qm} = 0$

Among these, rotor flux orientation is widely adopted due to its effectiveness in decoupling torque and flux, facilitating independent control. In our study, we employ rotor flux orientation for the dual three-phase induction machine.

By aligning the rotor flux along the d-axis ($\emptyset_{dr}$= $\emptyset_r$ $\emptyset_{qr}$= 0) , the electromagnetic torque C_{em} can be expressed as:

$$C_{em} = p\frac{L_m}{L_m+L_r}[(i_{qs1} + i_{qs2})\emptyset_{dr} - (i_{ds1} + i_{ds2})\emptyset_{qr}] \quad \text{(III.21)}$$

Given $\emptyset_{qr}$= 0 this simplifies to:

$$C_{em} = p\frac{L_m}{L_m+L_r}[(i_{qs1} + i_{qs2})\emptyset_r] = K''\emptyset_r i_q \quad \text{(III.22)}$$

This formulation mirrors the torque expression of a separately excited DC machine, where torque is the product of flux and armature current. Thus, under rotor flux orientation, the dual three-phase induction machine exhibits control characteristics akin to a DC machine with separate excitation [38].

III.4.4 Vector control methods:

The vector control technique applied to the dual three-phase induction machine can be categorized into direct and indirect control methods.

a) Direct control method:

This method involves determining both the position and magnitude of the flux, regardless of the operating regime. Two approaches are commonly used:

- Flux measurement in the air gap of the machine using a sensor. However, this technique has a significant limitation, as flux sensors are mechanically fragile.
- Flux estimation using mathematical models. This approach is susceptible to variations in machine parameters.

b) Indirect control method:

This method does not directly measure the amplitude of the rotor flux but instead uses its position. It does not require a rotor flux sensor, but it does necessitate the use of a position (or speed) sensor or an estimator for the rotor. A notable disadvantage of this method is the

sensitivity of the flux estimate to variations in machine parameters, which can be caused by magnetic saturation and temperature changes, particularly affecting the rotor time constant.

c) Speed control by the direct method:

In direct vector control, knowledge of both the magnitude and position of the rotor flux is crucial. To achieve this, an estimator for the rotor flux, denoted as φr, is derived from the stator current measurements. These currents are transformed into $ids1$, $iqs1$, $ids2$, $iqs2$, and the slip pulsation. The simplified block diagram of the flux-oriented control is depicted in Figure III.8.

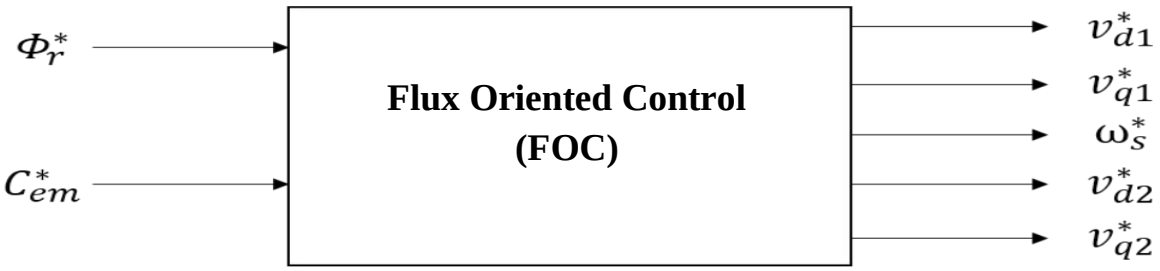

Figure III.8: Simplified schematic of flux-oriented control.

By applying the orientation of the rotor flux to the system equations (II.61) becomes:

$$I_{dr} = \frac{1}{L_m+L_r}[\emptyset_r - L_m(i_{ds1} + i_{ds2})] \quad \text{(III.23)}$$

$$I_{qr} = \frac{-L_m}{L_m+L_r}(i_{qs1} + i_{qs2}) \quad \text{(III.24)}$$

Substituting (2.3) and (2.4) in (I.42) we find

$$\begin{aligned} \emptyset_{ds1} &= \lambda_1 i_{ds1} + L_r \eta i_{ds2} + \eta \emptyset_r^* \\ \emptyset_{qs1} &= \lambda_1 i_{qs1} + L_r \eta i_{qs2} \\ \emptyset_{ds2} &= \lambda_2 i_{ds2} + L_r \eta i_{ds1} + \eta \emptyset_r^* \\ \emptyset_{qs2} &= \lambda_2 i_{qs2} + L_r \eta i_{qs1} \end{aligned} \quad \text{(III.25)}$$

With:

$$\eta = \frac{L_m}{L_m+L_r} ; \lambda_{1,2} = L_{s1,s2} + \eta L_r \quad \text{(III.26)}$$

And we have :

$$\emptyset_r^* = L_m(i_{ds1} + i_{ds2}) \quad \text{(III.27)}$$

$$I_{qr} = \frac{-\omega_{gl}\emptyset_r^*}{R_r} \qquad \text{(III.28)}$$

By replacing in the system of stator voltage equations (II.39), we obtain:

$$\begin{aligned} v_{ds1}^* &= R_{s1}i_{ds1} + L_{s1}\frac{d}{dt}i_{ds1} - \omega_s^*(L_{s1}i_{qs1} + T_r\emptyset_r^*\omega_{gl}^*) \\ v_{qs1}^* &= R_{s1}i_{qs1} + L_{s1}\frac{d}{dt}i_{qs1} - \omega_s^*(L_{s1}i_{ds1} + \emptyset_r^*) \\ v_{ds2}^* &= R_{s2}i_{ds2} + L_{s2}\frac{d}{dt}i_{ds2} - \omega_s^*(L_{s2}i_{qs2} + T_r\emptyset_r^*\omega_{gl}^*) \\ v_{qs2}^* &= R_{s1}i_{qs2} + L_{s2}\frac{d}{dt}i_{qs2} - \omega_s^*(L_{s2}i_{ds2} + \emptyset_r^*) \end{aligned} \qquad \text{(III.29)}$$

then:

$$i_{qs1}^* + i_{qs2}^* = \frac{(L_m+L_r)}{pL_m\emptyset_r^*}C_{em}^* \qquad \text{(III.30)}$$

$$\omega_{gl}^* = \frac{R_rL_m}{(L_m+L_r)\emptyset_r^*}(i_{qs1}^* + i_{qs2}^*) \qquad \text{(III.31)}$$

The torque equation reveals a coupling between the reference flux and the quadrature stator current components, indicating that they are not entirely independent. To enable independent control of torque and flux, it is essential to introduce decoupling variables that allow for their separate regulation.

$$\begin{aligned} v_{ds1l} &= R_{s1}i_{ds1} + L_{s1}\frac{d}{dt}i_{ds1} \\ v_{qs1l} &= R_{s1}i_{qs1} + L_{s1}\frac{d}{dt}i_{qs1} \\ v_{ds2l} &= R_{s2}i_{ds2} + L_{s2}\frac{d}{dt}i_{ds2} \\ v_{qs2} &= R_{s2}i_{qs2} + L_{s2}\frac{d}{dt}i_{qs2} \end{aligned} \qquad \text{(III.32)}$$

The system (III.15) implies that the stator voltages and currents are directly related. To compensate for the error introduced during decoupling, the reference stator voltages are introduced:

$$\begin{aligned} v_{ds1}^* &= v_{ds1l} - v_{ds1c} \\ v_{qs1}^* &= v_{qs1l} + v_{qs1c} \\ v_{ds2}^* &= v_{ds2l} - v_{ds2c} \\ v_{qs2}^* &= v_{qs2l} + v_{qs2c} \end{aligned} \qquad \text{(III.33)}$$

With:

$$v_{ds1c} = \omega_s^*(L_{s1}i_{qs1} + T_r\emptyset_r^*\omega_{gl}^*)$$

$$v_{qs1c}=\omega_s^*(L_{s1}i_{ds1}+\emptyset_r^*)$$
$$v_{ds2c}=\omega_s^*(L_{s2}i_{qs2}+T_r\emptyset_r^*\omega_{gl}^*) \quad \text{(III.34)}$$
$$v_{qs2c}=\omega_s^*(L_{s2}i_{ds2}+\emptyset_r^*)$$

To achieve effective decoupling, current regulation loops are introduced for the stator currents $i$ds1, $i$ds1, $i$qs1, $i$qs2. These control loops yield the corresponding stator voltage references V_{ds1}, V_{ds2}, V_{qs1}, V_{qs2} at their outputs [39].

III.5 Synthesis of PI controllers:

To enhance robustness against internal and external disturbances, Proportional-Integral (PI) controllers are employed. For systems characterized by a first-order transfer function[39]:

$$H(s)=\frac{1}{as+b} \quad \text{(III.35)}$$

The PI controller has the transfer function:

$$C(s)=K_p+\frac{K_i}{S} \quad \text{(III.36)}$$

Where Kp is the proportional gain and Ki is the integral gain. The closed-loop system, with unit feedback, is depicted in Figure III.9.

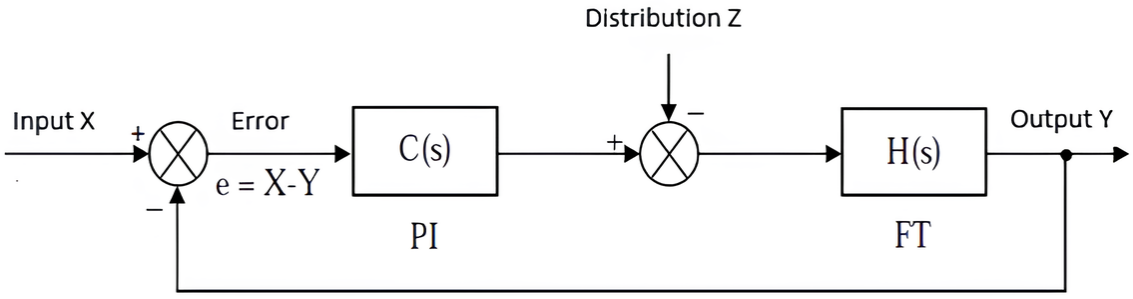

Figure III.09: First-order system with PI controller.

Neglecting disturbances during parameter identification, the open-loop transfer function becomes:

$$T(s)=C(s)H(s)=\frac{K_pS+K_i}{aS^2+bS} \quad \text{(III.37)}$$

The closed-loop transfer function is:

$$F(s) = \frac{T(s)}{1+T(s)} = \frac{K_p S+K_i}{aS^2+(K_p+b)S+K_i} \quad \text{(III.38)}$$

To achieve a desired first-order behavior:

$$G(s) = \frac{1}{rs+1} \quad \text{(III.39)}$$

It suffices to identify (II.24) with (II.25) as follows:

$$\frac{K_p S+K_i}{aS^2+(K_i+b)S+K_i} = \frac{1}{rs+1} \quad \text{(III.40)}$$

Which give:

$$aS^2 + (K_P + b)S + K_i = K_P\tau S^2 + (K_P + K_i\tau)S + K_i \quad \text{(III.41)}$$

$$K_p = \frac{a}{\tau} \quad \text{(III.42)}$$

$$K_i = \frac{b}{\tau} \quad \text{(III.43)}$$

III.5.1 Tuning parameters for current PI controllers:

The stator current control loop for phases (stars) 1 and 2 illustrated on Figure (III.10)

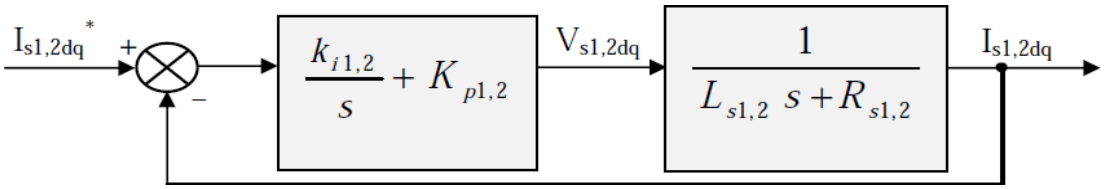

Figure III.10 : Stator current control loop.

With the relations:

$$K_{P1} = \frac{L_{s1}}{r} \quad \text{et} \quad K_{P2} = \frac{L_{s2}}{r} \quad \text{(III.44)}$$
$$K_{i1} = \frac{R_{s1}}{r} \qquad K_{i2} = \frac{R_{s2}}{r}$$

We take $r = \tau_r/6$ to ensure fast system dynamics, where $\tau r = Lr/Rr$ represents the electrical rotor time constant.

The voltage decoupling scheme (Field Oriented Control FOC) is represented in Figure III.11.

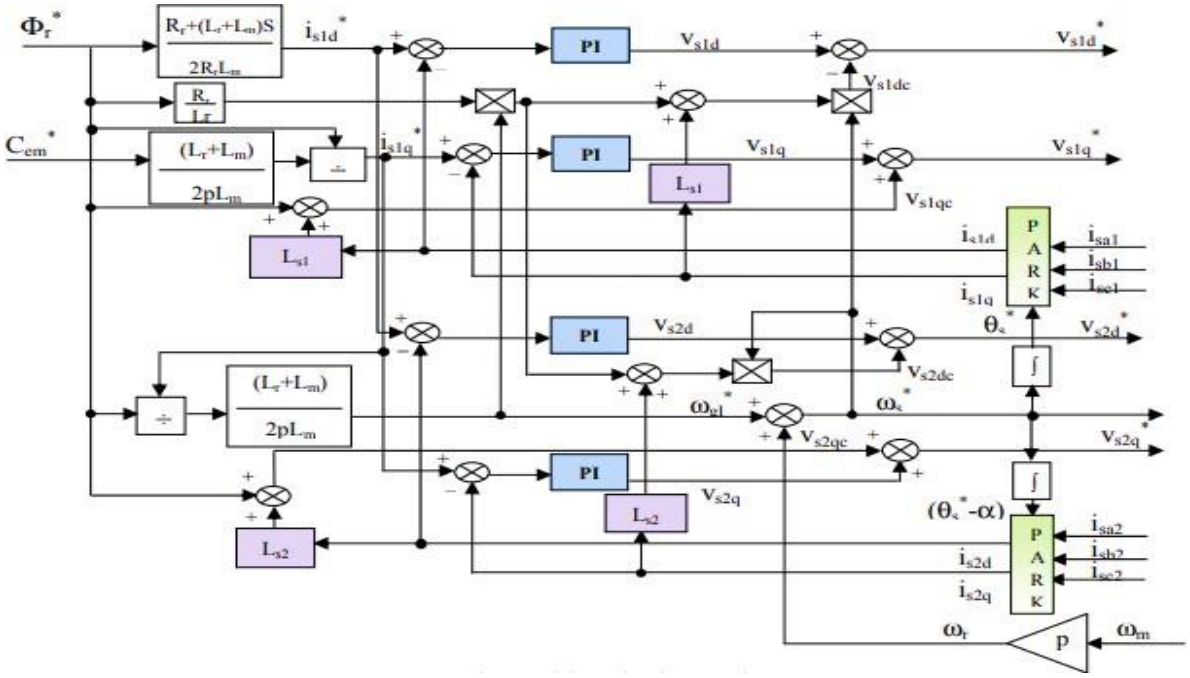

Figure III.11 : Voltage decoupling scheme.

III.5.2 Tuning parameters for speed PI controllers:

The speed control block diagram is presented in Figure (III.12).

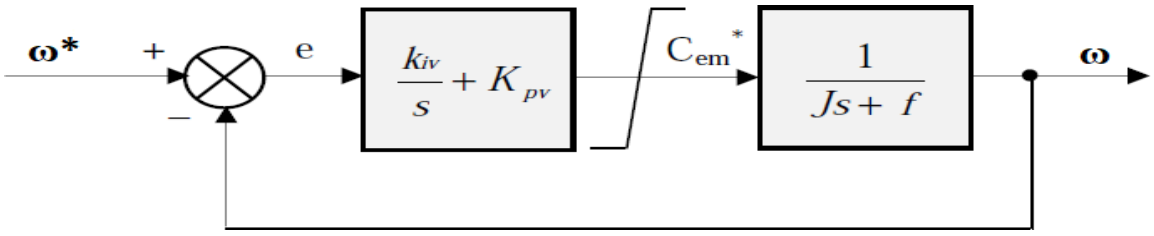

Figure III.12: Speed control diagram.

Using a similar method as for the current loop, we obtain:

$$K_{pv} = \frac{j}{r} \quad \text{(III.45)}$$

$$K_{iv} = \frac{f}{r} \quad \text{(III.46)}$$

With: $r = r_r$.

The torque command is constrained by a saturation block defined by:

$$C_{em}^{*} = C_{em}^{*} si |C_{em}^{*}| \leq C_{em}^{max}$$

$$C_{em}^{max} \text{signe}(C_{em}^{*}) \text{Si} |C_{em}^{*}| \geq C_{em}^{max} \quad \text{(III.47)}$$

III.6 Flux weakening control:

The field weakening strategy adjusts the rotor flux reference directly from the measured rotor speed using a speed sensor. A nonlinear flux reference characteristic is implemented as follows [40].

$$\emptyset_{\text{rref}} = \emptyset_{\text{n}} \text{si} |\Omega| \leq \Omega_{\text{n}} \quad \text{(III.48)}$$

$$\emptyset_{\text{rref}} = \emptyset_{\text{n}} = \frac{\Omega_{\text{n}}}{\Omega} \text{si} |\Omega| > \Omega_{\text{n}} \quad \text{(III.49)}$$

Figure III.13 illustrates the field weakening control graph. Below the nominal speed ωn, the flux is held at its rated value φn. Above ωn, the flux is reduced in inverse proportion to the speed to limit the machine terminal voltage.

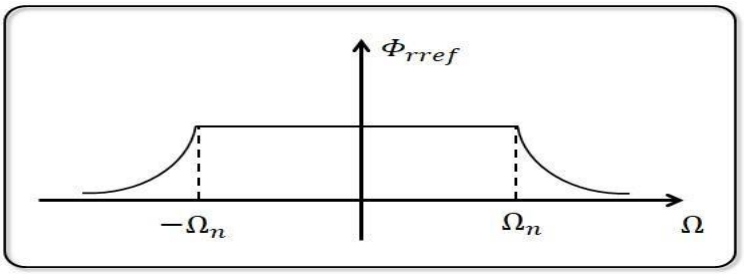

Figure III.13 : Field weakening control graph.

Below the nominal speed ωn, the rotor flux is held at its rated value φn. For |ω|>ωn , the flux reference is reduced inversely with speed to keep the machine's terminal voltage within allowable limits.

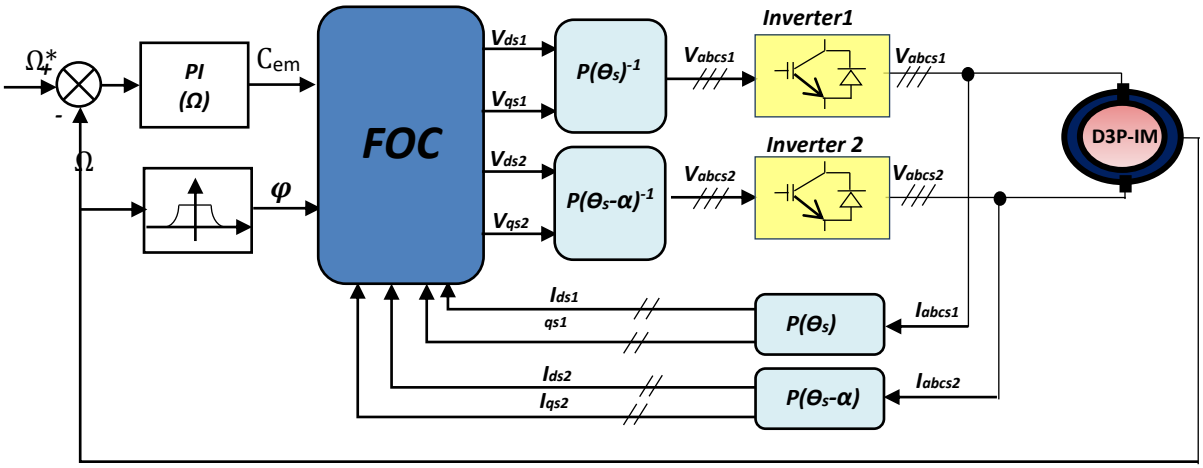

Figure III.14: Field-oriented control with field weakening for the dual three-phase induction machine

III.7 Simulation and results:

The dual three-phase induction machine was simulated under indirect vector control with speed regulation. Three operating scenarios were tested:

- **Startup and No-Load:**
  - A reference speed is reached by $t \approx 0.73$ s.
  - The electromagnetic torque *Cem* peaks at 68.5 N·m at $t = 0.049$ s, then damps out by $t \approx 0.75$ s, settling near zero due to friction.
  - Stator currents (stars 1 and 2) exhibit an initial inrush (~2× rated current) before settling into steady-state sine waves.
  - The quadrature-axis current *iqs1* mirrors the torque pulse, rising to ~12 A during the transient and returning to zero in steady-state.
  - Rotor flux linkages follow the torque profile during transients and then hold their commanded values in steady-state.
- **Applied Load of +14 N·m (t = 1.5 – 2s)**
  - Torque, stator currents, and rotor flux rise and then stabilize at Cem= +14 N·m, *ias1*= *ias2*= 6.2 A, and *iqs1*= 7.0 A.
  - Rotor speed remains at its setpoint, and flux linkages remain undisturbed.
- **Applied Load of –14 N·m (t = 4– 4. 5 s)**
  - Torque reverses and settles at *Cem*= –14 N·m, with *ias1*= *ias2*= 6.2 A, and *iqs1*= –7.0 A.
  - Speed and rotor flux remain fixed at their commanded values.
  - The supply voltage *Vas1* and current *ias1* remain almost in phase, indicating positive active power flow into the machine; a slight current lag persists due to inductance.
- **Speed Reversal (+300 → –300 rad/s at *t* = 2. 5 s)**
  - The rotor speed tracks the new reference and reverses direction by ~1.10 s.
  - Stator currents again surge to ~2.5× rated during the reversal transient, then settle into steady sine waves by $t \approx 3.6$ s.
  - Torque transitions to –14 N·m and stabilizes.
  - The quadrature current *iqs1* follows the torque reversal, and both d- and q-axis rotor flux linkages show only minor disturbances during the inversion.

These results confirm that the indirect vector control scheme ensures accurate speed tracking, fast torque response, and robust handling of load changes and reversals.

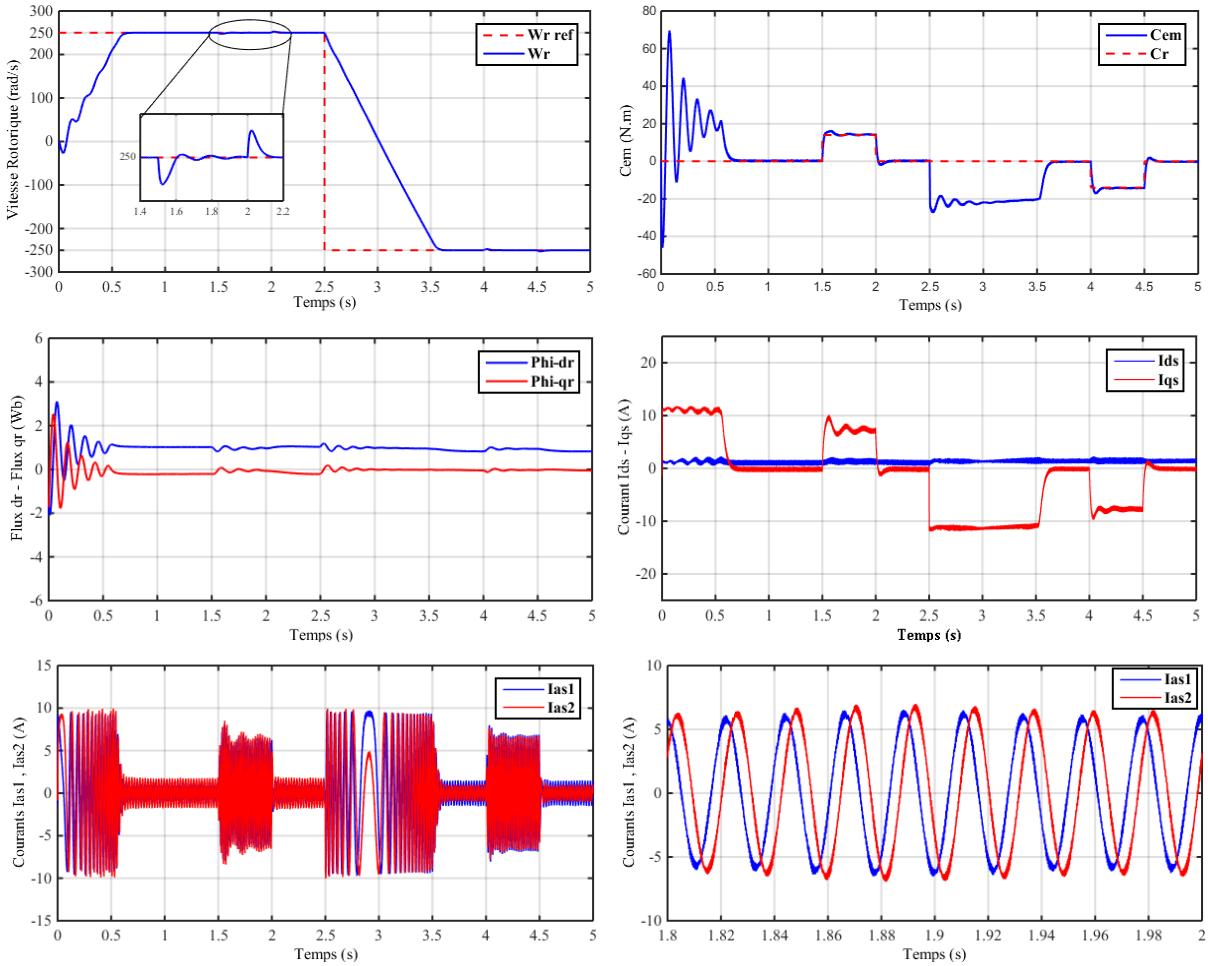

Figure III.15: Speed control of the dual three-phase induction machine by indirect method based on PI controllers

- **Robustness Test :**

In order to test the robustness of the rotor flux orientation vector control with the indirect method, two tests are carried out. The first is that of the variation of the rotor resistance and the second test for the variation of the stator resistance.

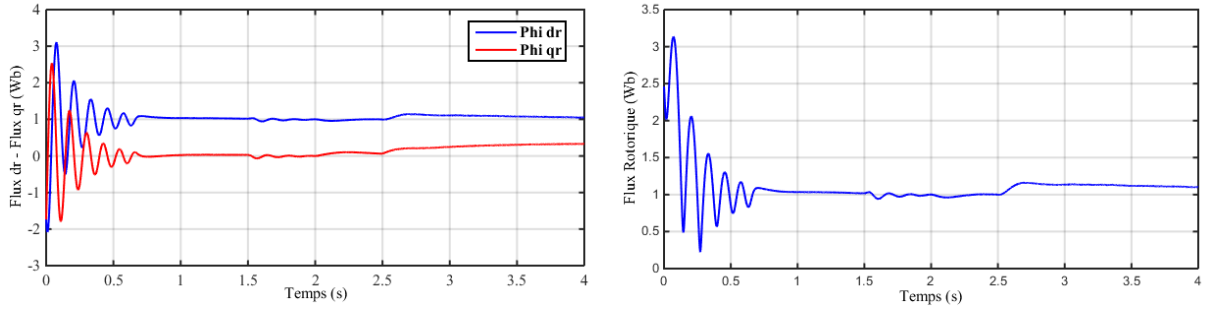

Figure III.16: Robustness test for a variation of +50% of the stator resistance, for the speed of the D3P-IM (under a nominal load) by indirect vector control.

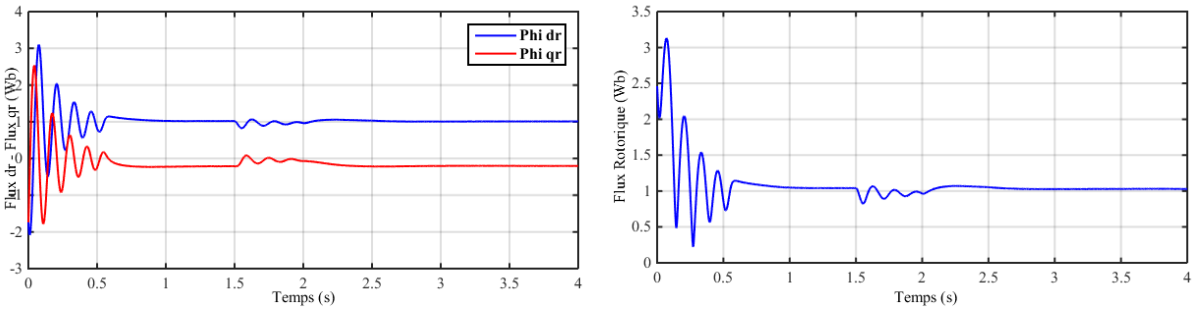

Figure III.17: Robustness test for a variation of +50% of the stator resistance, for the speed of the D3P-IM (under a nominal load) by indirect vector control.

Figure III.16 represents the evolution of the D3P-IM characteristics with the speed regulation by the indirect method, followed by the increase of the rotor resistance by 50% at time t = 2.5s with the application of loads Cr = 14N.m in the time interval t = [1.5; 2]s, while imposing the reference speed ωr*= 300rad/s. These characteristics show, firstly, a slight variation in the speed due to the application of the load, secondly, stability in the evolution of the current (i_{as1} (A)) and the rotor flux, finally a slight disturbance caused mainly by the increase in the rotor resistance at the level of the direct and quadrature rotor fluxes.

Figure III.17 shows the evolution of the D3P-IM characteristics with speed regulation by the indirect method, followed by the increase in stator resistance of 50% at time t = 2.5s with the application of loads Cr = 14N.m in the time interval t = [1.5; 2]s, while imposing the reference speed ωr*= 300rad/s.

The variation in stator resistances is not taken into account by the control system, even if the machine under control is no longer the machine considered by the control.

III.8 Conclusion:

This chapter focused on the implementation of vector control based on rotor flux orientation for the dual three-phase induction machine, with the primary objective being speed regulation through the indirect control method. Through this study, we effectively highlighted the dynamic behavior and performance characteristics offered by vector control when applied to multiphase machines. The simulation results confirmed that indirect vector control allows for precise decoupling of torque and flux, leading to improved transient and steady-state responses.

Despite these advantages, further enhancement in performance can be achieved by replacing conventional PI controllers with ANN controllers. Consequently, the next chapter is dedicated to exploring the integration of ANNs controllers with the dual three-phase induction machine to optimize control precision, enhance the robustness, and further improve the overall system efficiency.

CHAPTER IV

Field Oriented Control of Dual Three-Phase Induction Machine Based on ANN Controllers

IV.1 Introduction:

Artificial intelligence techniques are currently well known for their great potential for solving problems linked to industrial processes, in particular the control, estimation and identification of variant system parameters. Among these techniques are fuzzy logic and neural networks, which are increasingly being applied to the control of induction machines and the adaptation of their vector control.

In this chapter, a description of artificial neural network techniques and their application to the control of the double-star asynchronous machine is presented. Simulation results are also presented to demonstrate the effectiveness of this technique in solving the problem of robustness to variations in D3P-IM parameters.

IV.2 Vector control using artificial neural networks:

IV.2.1 Artificial neural networks:

The origins of Artificial Neural Networks (ANNs) lie in attempts to model the human brain mathematically. The earliest work dates back to 1943 and was carried out by Mac Culloch and Pitts. They assumed that the nerve impulse is the result of a simple calculation performed by each neuron, and that thought arises through the collective effect of a network of interconnected neurons. They had a promising start in the late '50s, but the lack of further development of the theory froze this work until the '80s [41].

a) Biological neuron:

The neuron is a cell composed of a cell body and a nucleus. The information processed by the neuron then travels along the (single) axon to be transmitted to other neurons. Transmission between two neurons is not direct. In fact, there is an intercellular space of a few tens of Angstroms between the axon of the afferent neuron and the dendrites of the efferent neuron. The junction between two neurons is called the synapse, and figure IV.10 shows a biological neuron [42].

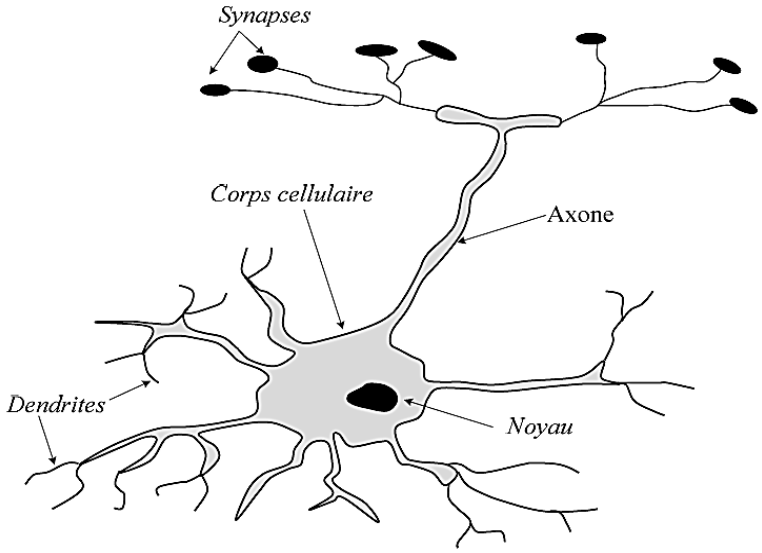

Figure IV.1 Simplified diagram of a biological neuron.

The biological neuron (Figure IV.1) comprises :

- **The cell body**, which sums up the influxes it receives; if this sum exceeds a certain Bias, it itself sends an influx via the axon ;
- **The axon**, which transmits signals from the cell body to other neurons ;
- **The dendrites**, which are the neuron's main receptors, picking up incoming signals ;
- **Synapses**, which enable neurons to communicate with others via axons and dendrites.

b) Formal (artificial) neuron:

The formal neuron is a very simple mathematical model designed to reproduce “intelligent” reasoning in an artificial way, such as summation and comparison. Each formal neuron calculates a single output based on the information it receives.

Figure IV.2 shows the structure of an artificial neuron. Each artificial neuron is an elementary processor. It receives a variable number of inputs from "upstream" neurons. Each of these inputs is associated with a weight w, representing the strength of the connection. Each elementary processor has a single output, which then branches out to feed a variable number of "downstream" neurons. Each connection is assigned a weight [41] [42].

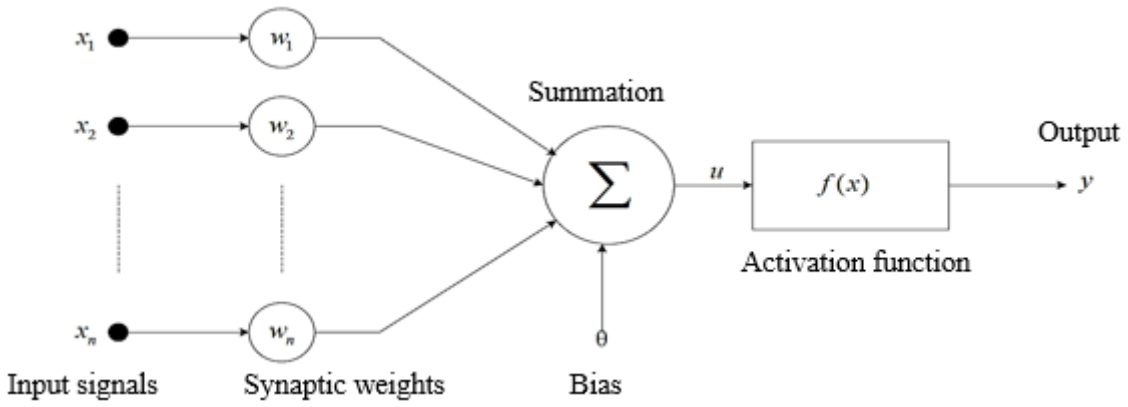

Figure IV.2 Formal neuron modeling.

Each neuron is connected to different inputs (x_n). These are either the input variables of the network, or the outputs of previous layers. Each of these inputs is weighted by a weight (w_i). A total weight (S) is thus calculated after adding the bias (β) specific to each neuron. This weight, normalized between -1 and 1, indicates the neuron's degree of activation. A sigmoid function (f) is then used to propagate the information, giving an output (y) always normalized between -1 and 1 .

All the information is then stored in the value of the weights, and a back-propagation learning algorithm, based on numerous examples, is required to optimize a solution.

The formal neuron is therefore a Boolean automaton whose output (y) is such that:

$$y = \begin{cases} 1 & si \quad S > \beta \\ 0 & si \quad S < \beta \end{cases} \qquad \text{(IV.1)}$$

with :

$$y = f(x) \; et \; S = \sum_{i=1}^{n} w_i . x_i \qquad \text{(IV.2)}$$

The quantities involved in relation (IV.2) are defined as follows :

x_i : Represents the ith input of the formal neuron .

y : Neuron output .

β: Neuron bias .

w_i: Weighting parameters .

f: Thresholding function .

S: Weighted sum of inputs xi .

The table below shows the mapping between a biological neuron and an artificial neuron:

Biological neuron	***Artificial neuron***
Synapses	Weight of connections
Axons	Output signal
Dendrites	Input signal
Nucleus or Somma	Activation function

Table IV.1 Analogy between biological and artificial neurons.

In more general terms, the formal neuron can be defined by the following elements [43].

1 -Inputs to the neural network: These can be binary (0, 1) or real .

2 -Activation function: This function defines the neuron's internal state as a function of its total input :

-Linear function: This is one of the simplest activation functions, defined by: $f(x) = x$, (Figure IV.3) .

- Sigmoid function: This is the continuous equivalent of the linear function. Being continuous, it is derivable, especially as its derivative is simple to calculate (Figure IV.4). It is defined by:

$$f(x) = \frac{1}{1+e^{-x}} \qquad \text{(IV.3)}$$

3- Output function: Calculates the output of a neuron as a function of its activation state. In general, this function is considered to be the identity function. It can be binary (0, 1), bipolar (-1, 1) or real.

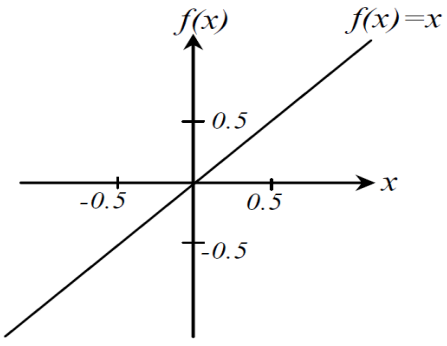

Figure IV.3 Linear function.

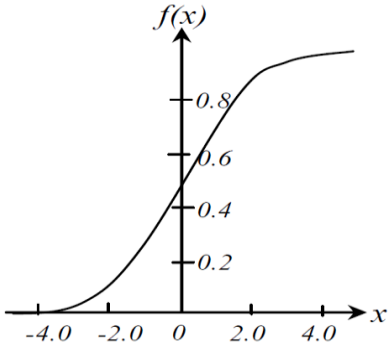

Figure IV.4 Sigmoid function.

c) Connection weights:

A weight w_{ij} is associated with each connection. We will always denote the first index by i and the second by j. The first index (row) designates the neuron number on the layer, while the second index (column) specifies the input number. Thus, w_{ij} designates the weight of the

connection linking neuron *i* to its input *j* [44].

The weight of an artificial neuron thus represents the efficiency of a synaptic connection. A negative weight inhibits an input, while a positive weight accentuates it.

d) Neural network learning:

Two essential features of neural networks are learning and adaptation. The role of learning is to define the weight of each connection. Numerous rules exist for modifying the weight of connections and thus achieving correct learning [44]. When the learning phase is complete, the network must be able to make the right associations for input vectors it has not learned. This is one of the most important properties of neural networks, as it provides the ability to recognize similar and even degraded forms of the prototypes - the recognition phase.
Learning algorithms perform best when provided with multiple and varied examples, so the network can assimilate all the knowledge. There are a number of different learning rules:

- **Supervised learning :**

A supervisor, or teacher, provides the network with input-output pairs. He teaches the network to learn all these pairs, using a learning method such as error gradient backpropagation, by comparing the actual output of the network with the desired output for each pair. Learning is complete when all input-output pairs are recognized by the network. This type of learning, illustrated in figure IV.14, can be found, among others, in the perceptron [42].

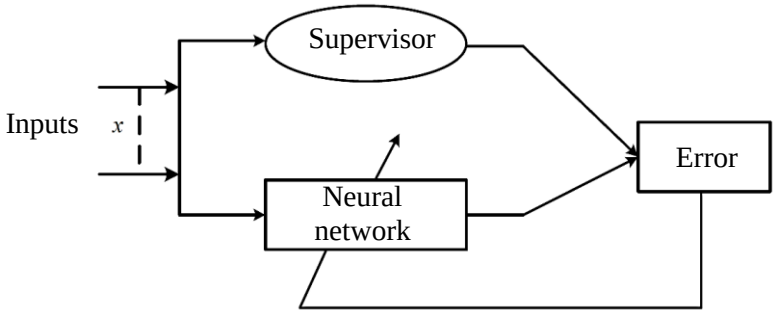

Figure IV.5 Illustration of supervised learning.

- **Non-supervised learning :**

Non-supervised learning consists in automatically detecting regularities in the examples presented, and modifying the weights of the connections so that examples with the same regularity characteristics produce the same output. Kohonen's self-organizing networks are the best-known unsupervised learning networks, as shown in figure IV.6 [42].

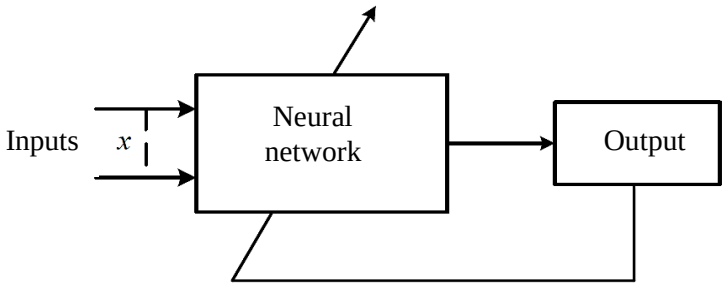

Figure IV.6 Illustration of non-supervised learning.

- **Auto-supervised learning :**

The neural network evaluates its own performance, without the help of a "teacher". An object is presented to the input of the neural network, which is told which class it belongs to. If the network doesn't classify it correctly, it measures the error itself, and propagates this error to the input. The network performs as many iterations as necessary until it obtains the correct answer.

IV.2.2 Neural network application to vector control of the D3P-IM:

A well-designed neural network controller can provide better control performance. In the literature, it has been concluded that a neural network with a single hidden layer can approximate any process. However, certain parameters of ANNs cannot be determined from a theoretical analysis of the process, such as the number of neurons and activation functions. As a result, it is important to note that only experience and the number of tests carried out can determine the number of neurons or, more precisely, the optimal architecture for a given problem.

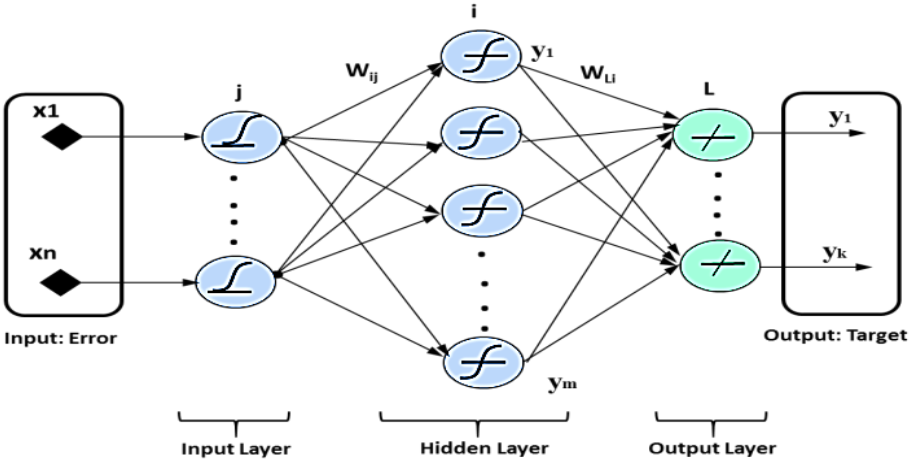

Figure IV.7 Standard neural network structure.

The general structure illustrated in Figure IV.7, consists of three layers, input-output, and a hidden layer with n, k, and m neurons, respectively.

The signal propagation of each layer is described in detail as follows:

$$u_j = X(j)\,(j=1,2,\cdots n) \tag{IV.4}$$

Where, u_j denotes the j^{th} neuron used for the input layer, and the number n of neurons depends on the complexity of the process.

The input and output of the hidden layer are:

$$v_i = \sum_{j=1}^{n} \omega_{ij} u_j \tag{IV.5}$$

$$y_i = f(v_i) = f\left(\sum_{j=1}^{n} \omega_{ij} u_j\right)\left(i = 1,2,\cdots m\right) \tag{IV.6}$$

Where, y_i is the total input of the i^{th} neuron used for the hidden layer, w_{ij} is the weight values, and $f(*)$ designates the activation function.

The input to the output layer is:

$$z_L = \sum_{L=1}^{k} \omega_{Li} y_i = \sum_{L=1}^{k} \omega_{Li} f(v_i) \tag{IV.7}$$

The total output of the neural network can be represented by the following equation:

$$y_k = f\left(z_L\right) = f\left(\sum_{L=1}^{k} \omega_{Li} f\left(v_i\right)\right) = f\left(\sum_{L=1}^{k} \omega_{Li} f\left(\sum_{j=1}^{n} \omega_{ij} u_j\right)\right) \tag{IV.8}$$

Based on self-structuring, the optimal MLP architecture proposed in this work is composed of a single-neuron input layer, a three-neuron hidden layer and a single-neuron output layer, to realize the RNA controllers that replace the four conventional PI current controllers, in order to maintain high dynamic performance even under parametric variation. First, we train the MLP to the PI controller by presenting 60000 samples to the network with a maximum error of 10^{-20}, with a maximum number of epochs of 103 and an iteration step of five. Next, the MLP must be trained to adjust and find the appropriate weights, which adapt the input (error) to the output (target). The activation functions for the input and output layers are the "**logsig**" and '**tansig**' functions respectively, while the "**linear**" function is used for the output layer. Its training is carried out using the error-based gradient propagation algorithm, which is chosen by one of the fastest algorithms for training MLPs of moderate size and ensures the best convergence towards a minimum of squared error.

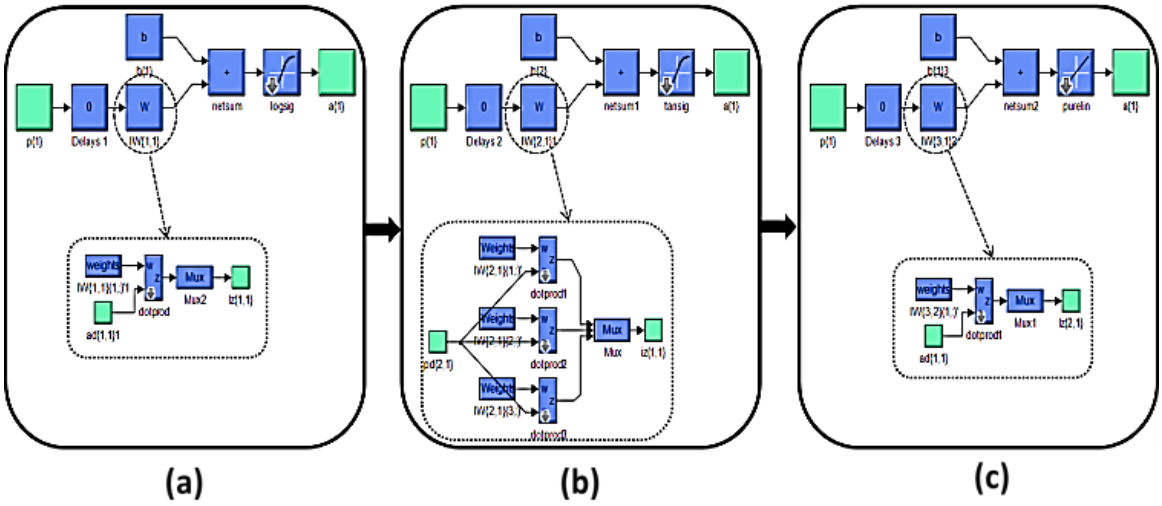

Figure IV.8 Block diagram of a digital controller: (a) Input layer; (b) Hidden layer; (c) Output layer.

Each neuron in this architecture has a corresponding Bias b, as shown in Figure IV.8

The adaptation of weight and Bias values can be represented by the following equations:

$$\xi_i(k+1) = \xi_i(k) + \Delta\xi_i \qquad \text{(IV.9)}$$

$$\Delta\xi_i = -\eta \frac{\partial\varepsilon(k)}{\partial\xi_i(k)} \qquad \text{(IV.10)}$$

with: $\xi_i = w_i$ or b_i.

$$\varepsilon(k) = \frac{1}{2}\sum_{i=1}^{m} e_i^{\,2}(k) \qquad \text{(IV.11)}$$

$$e_i(k) = y_{i\_desird} - y_{i\_actually} \qquad \text{(IV.12)}$$

Where, ***ε(k)*** is the instantaneous sum of the SSE output squared errors, ***e(k)*** is the error**,** ***η*** is a learning rate that takes a constant value between 0 and 1. The initial values of the weights and Bias are chosen randomly.

The general parameters (number of layers, maximum error, activation functions) can be successfully applied in other applications, as shown in the literature [45, 46]. However, the appropriate design parameters (number of neurons, weight values, Bias values) can only be applied successfully in the same applications. Indirect vector control with the artificial neural network application for D3P-IM is illustrated in Figure IV.9.

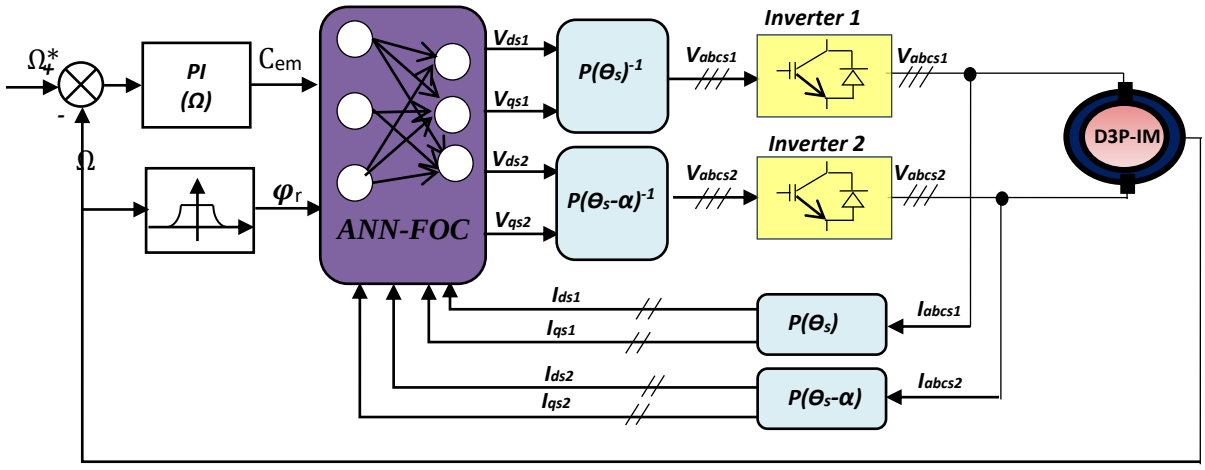

Figure IV.9 Functional diagram of the FOC-RNA proposed for D3P-IM.

IV.3 Interpretation of simulation results for neural network-based vector control:

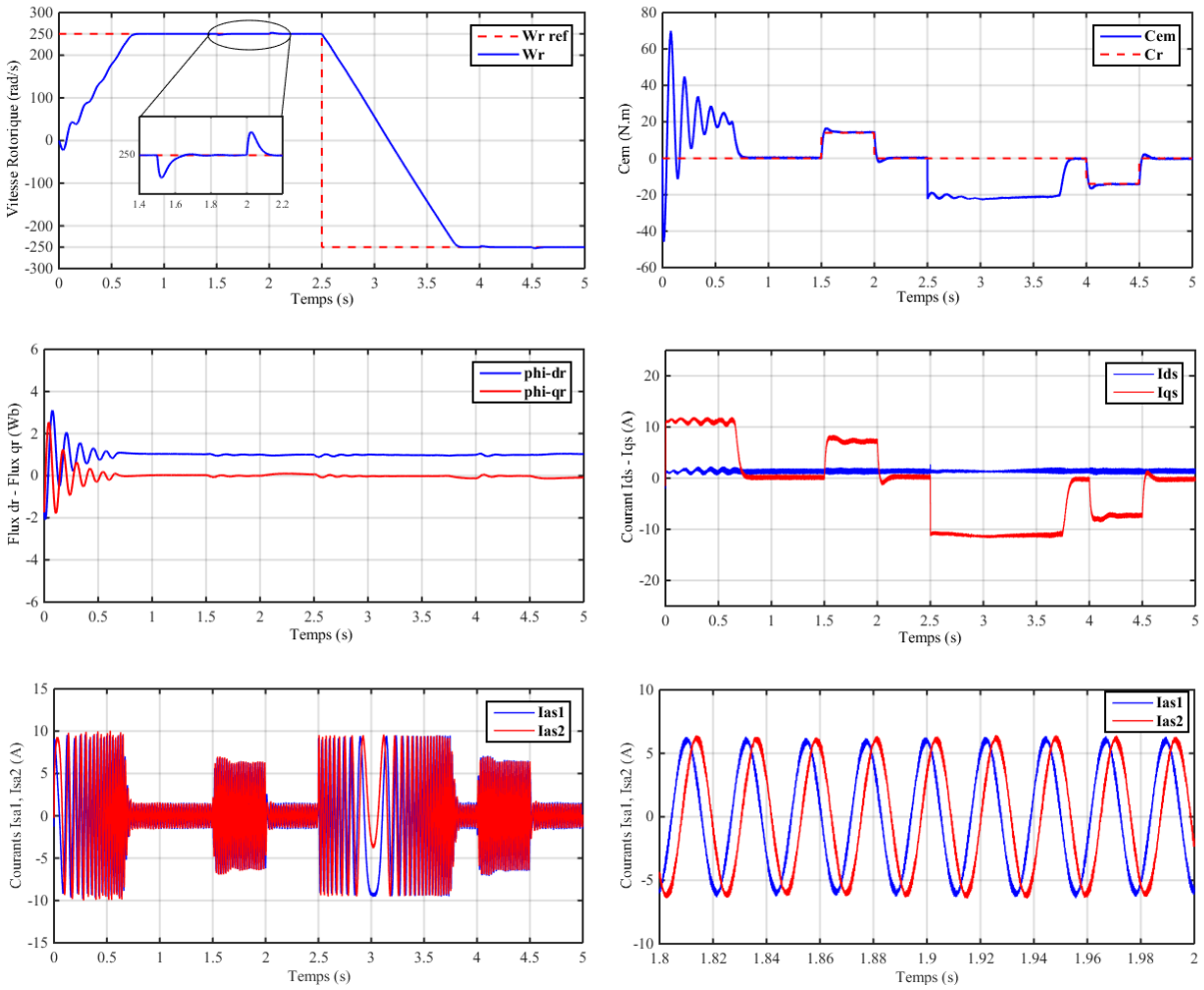

Figure IV.10 Evolution of D3P-IM characteristics during neural network-based vector control.

Figure IV.10, shows the evolution of the neural network-based vector control characteristics applied to the D3P-IM, followed by speed inversion from 300 to -300 from time t = 2.5s and application of loads Cr = 14 Nm in time interval t = [1.5 ; 2] s
and Cr = -14Nm in t =[4 ; 4.5]s.

At start-up and during transient operation, speed increases linearly with time, reaching its reference value at t = 0.6s without overshooting. The electromagnetic torque reaches its maximum value at start-up, then reaches steady state at t = 0.6s. Initially, the stator current ias1 reaches an inrush current of around 10A. The quadrature current initially reaches 11A, after which it evolves identically to the electromagnetic torque. The rotor fluxes according to (d, q) show peaks for a fraction of a second at start-up, oscillating around their setpoints. However, the same results as for PI control are obtained with neural network control. Nevertheless, with better speed regulation (accuracy, stability and speed) by the neural network control technique.

After t = 2.5s, the speed reverses and reaches its negative setpoint after t = 1.2s, with no overshoot. This generates an increase in the ias1 current of a magnitude equal to that recorded during start-up, which stabilizes after 1.2s to give rise to the steady-state form.

The electromagnetic torque reaches its maximum value at the moment of speed reversal, which stabilizes as soon as the speed reaches its reference value (-300 rad/s), the quadrature current iqs1 increases in a similar way to the electromagnetic torque, and the rotor fluxes along the axes (d, q) follow their reference values during speed reversal.

- **Robustness tests :**

In order to test the robustness of the neural network control, two tests are carried out. The first test is for the variation of the rotor resistance, the second test for the variation of the stator resistance.

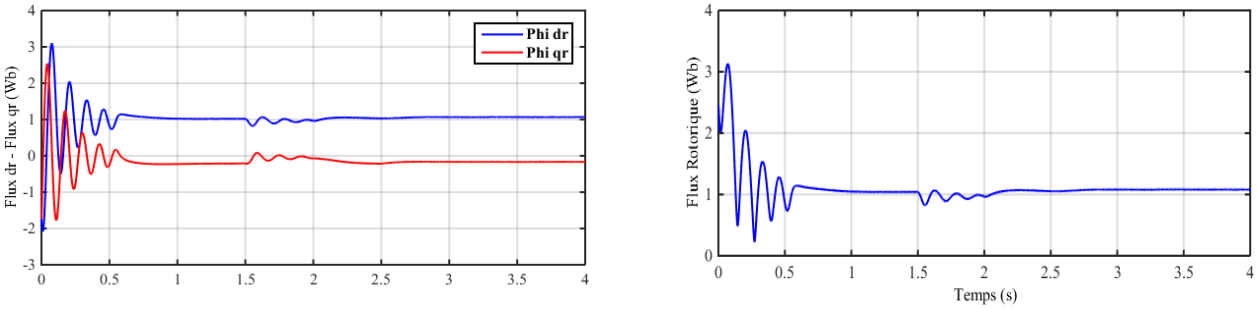

Figure IV.11 Robustness test for a +50% variation in rotor resistance, for D3P-IM speed control (under nominal load) by neural network-based vector control.

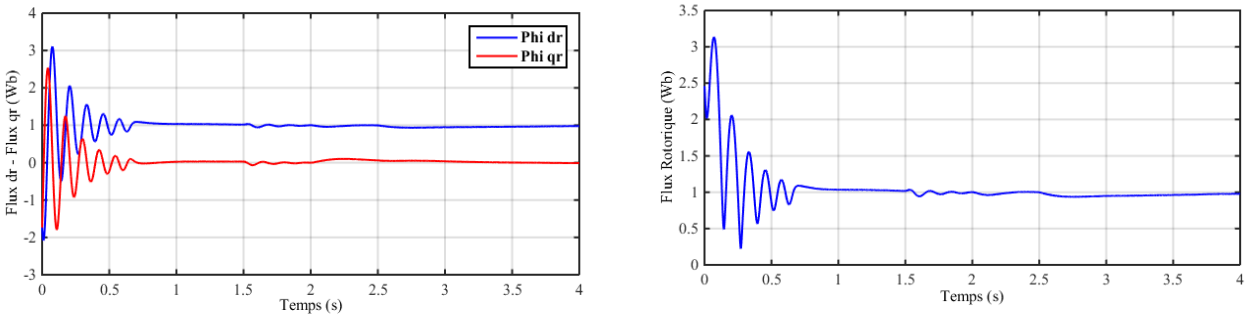

Figure IV.12 Robustness test for a +50% variation in stator resistance, for speed control of the D3P-IM (under nominal load) by neural network-based vector control.

Figure IV.11 shows the evolution of D3P-IM characteristics with neural network-based vector control, followed by a 50% increase in rotor resistance at time t = 2.5s with the application of loads Cr = 14N.m in the time interval t = [1.5 ; 2]s, while imposing the reference speed ωr^*= 300rad/s.

We note that a slight disturbance is observed by the rotor fluxes, which is due to the simultaneous effect of the variation in rotor resistance and load (Cr = 14N.m), as from t = 2.5s they resume their progressions according to their setpoints without disturbance.

Figure IV.12 shows the evolution of D3P-IM characteristics with neural network-based vector control, followed by the 50% increase in stator resistance at time t = 2.5s with the application of Cr = 14N.m loads in the time interval t = [1.5; 2]s, while imposing reference speed ωr^*= 300rad/s.

Simulation results clearly show the insensitivity of the neural network-based vector control to variations in stator and rotor resistance.

IV.4 Conclusion:

This chapter presented a detailed overview of artificial neural networks and their main topologies. A comparison between classical control and the proposed algorithm highlighted the benefits of increasing voltage levels. The ANN-FOC algorithm showed better output current quality, reduced harmonic distortion, and improved control performance. These advantages make it a more efficient and reliable choice for applications requiring high power quality. Overall, ANN controllers prove to be more suitable than PI controllers in advanced control systems.

General conclusion

This thesis has focused on the modeling, control, and performance enhancement of the dual three-phase induction machines control, with the primary goal of improving speed regulation and dynamic performance through advanced vector control techniques. This study investigated both traditional PI controllers and more advanced ANN controllers to assess the performance, robustness, and efficiency of the proposed control strategies.

The key outcomes of the study can be summarized as follows:

- **Chapter I** provided an overview of multiphase drive systems, with particular attention to dual three-phase induction machine. The unique advantages of these machines including enhanced fault tolerance, reduced per-phase current, and improved torque density, were highlighted, along with their growing application in high-power industrial sectors.
- **Chapter II** focused on the mathematical modeling of the dual three-phase machine. A dynamic model was developed using Park's transformation, taking into account a 30° phase shift between the stator windings. This representation was essential for implementing control strategies and understanding the machine's behavior under various operating conditions.
- **Chapter III** implemented vector control of the dual three-phase machine using field orientation control (FOC) supplied by two-level inverters. Simulation results demonstrated satisfactory control performance, with reduced torque ripple and improved current regulation compared to conventional three-phase machines.
- **Chapter IV** extended the control approach by integrating ANN controllers. A comparative analysis revealed that the proposed ANNs algorithm significantly enhance output waveform quality, and provide smoother torque control, affirming their suitability for high-performance industrial drives.

In summary, the work carried out in this thesis confirms the feasibility and effectiveness of using artificial neural network-based vector control for dual three-phase induction machines. Compared to conventional approaches, ANN controllers demonstrate clear advantages in terms of torque smoothness and control precision. These results position ANN-based control as a promising solution for the development of next-generation, high-performance industrial drive systems.

Building on the outcomes of this thesis, several potential directions for future research can be proposed to further advance the control and performance of dual three-phase induction machines:

- Extension to multilevel inverter topologies, such as cascaded H-bridge or flying capacitor structures, which could offer enhanced output waveform quality, improved fault tolerance, and higher efficiency compared to two-level inverters;

- Integration of advanced control strategies, including model predictive control (MPC), sliding mode control, or hybrid approaches combining fuzzy logic and neural networks, to further improve system robustness and dynamic performance under variable load and speed conditions;

- Experimental validation and hardware implementation of the proposed ANN-based vector control strategies, in order to confirm their effectiveness in real-time applications and to identify potential practical limitations or areas for optimization.

REFERENCES

[1] **E. Levi, R. Bojoi, F. Profumo, H. Toliyat, and S. Williamson,** "Multiphase induction motor drives – a technology status review," IET Electric Power Applications, vol. 1, no. 4, pp. 489–516, Jul. 2007.

[2] **M. A. Rahman, A. M. Osheiba, and M. Azizur Rahman,** "Advancements in multiphase motor drive technology," IEEE Transactions on Industrial Electronics, vol. 63, no. 1, pp. 25–36, Jan. 2016.

[3] **P. C. Krause**, **O. Wasynczuk**, **S. D. Sudhoff**, and **S. Pekarek**, *Analysis of Electric Machinery and Drive Systems*, 3rd ed. Hoboken, NJ, USA: Wiley-IEEE Press, 2022.

[4] **E. Levi**, "Multiphase electric machines for variable-speed applications," *IEEE Trans. Ind. Electron.*, vol. 55, no. 5, pp. 1893–1909, May 2008.

[5] **M. Jones**, **E. Levi**, and **S. N. Vukosavic**, "Fault tolerant control of five-phase induction machines with combined voltage- and current-fed excitation," *IEEE Trans. Ind. Electron.*, vol. 54, no. 1, pp. 174–186, Feb. 2007.

[6] **A. Kadaba**, "Design and modelling of a reversible 3-phase to 6-phase induction machine," M.S. thesis, Dept. Elect. Comput. Eng., Marquette Univ., Milwaukee, WI, USA, 2008.

[7] **D. J. O'Brien**, "Multiphase induction motor drives: A technology status review," *Inst. Eng. Technol. (IET)*, 2019.

[8] **M. P. Kazmierkowski**, **L. Malesani**, **A. Kasic**, and **A. Boglietti**, "Current control methods for an asymmetric six-phase permanent magnet synchronous motor," *Electronics*, vol. 9, no. 1, p. 172, Jan. 2020.

[9] **E. Levi**, **M. Jones**, **S. N. Vukosavic**, and **H. A. Toliyat**, "Steady-state modeling of multiphase induction machines with harmonic injection using vector space decomposition," *IEEE Trans. Energy Convers.*, vol. 19, no. 3, pp. 469–475, Sept. 2004.

[10] **S. D. Round**, **R. M. Duke**, and **S. D. Round**, "Development of a vector space decomposition model for a six-phase induction machine," in *Proc. IEEE Int. Symp. Ind. Electron.*, 2000, pp. 74–79.

[11] **Mohammed Hechelef**, Direct Torque Control of a Double Star Asynchronous Machine without Mechanical Sensor Using Artificial Intelligence Techniques, 2017.

[12] **Mohamed Said Bilal** and **Salah Eddine Berrabah**, Nonlinear Control of a Double Star Asynchronous Machine "MASDE", 2019.

[13] **BOUKHTACHE Seyfeddine** and **MESSINI Merouane**, Field Oriented Control of Induction Motors Based on DSP Controller, 2016.

[14] **Noureddine Layadi**, Fault-Tolerant Control of the Double Star Asynchronous Machine, 2020.

[15] **DIEDHIOU Tidjini**, Estimation of Speed and Stator and Rotor Resistances for Field-Oriented Control of an Asynchronous Machine, 2018.

[16] **SOUSSA Chems eddine , Walid ABADI , Houcine GABOUSSA and Abdalgalil HECHIFA**, Sliding Mode Control of the Double Star Asynchronous Machine, 2022.

[17] **Selatna Hamza , Selatna Hichem** and **Hechifa Abdelhak**, High Performance Control of a Six-Phase Induction Machine Using Multilevel converters, 2023.

[18] **G. K. Singh**, "Multi-phase induction machine drive research—A survey," *Elect. Power Syst. Res.*, vol. 61, no. 2, pp. 139–147, 2002.

[19] **L. Wogi**, **A. R. Thelkar**, **T. Tahiro**, and **S. Larguech**, "Particle swarm optimization based optimal design of six-phase induction motor for electric propulsion of submarines," *Energies*, vol. 15, no. 9, p. 2994, 2022.

[20] **P. Thirugnanam**, "Advances, new perspective and applications in induction motors," in *Induction Motors—Recent Advances, New Perspectives and Applications*, **A. El-Shahat**, Ed. London, U.K.: IntechOpen, 2023.

[21] **E. Levi**, **M. Jones**, and **S. N. Vukosavic**, "Multi-phase electric machines for aerospace applications," in *Proc. IEEE Int. Conf. Electr. Mach. Drives (IEMDC)*, 2007, pp. 41–48.

[22] **J. J. Listwan** and **P. Oleszczyszyn**, "Analysis of the drive of the electric vehicle with six-phase induction motor," *Power Electron. Drives*, vol. 8, no. 43, pp. 252–274, 2023.

[23] **A. Iqbal** and **S. M. Islam**, "Six-phase induction motor drive for oil and gas industry," in *Proc. IEEE Int. Conf. Power Eng. Optim. (PEOCO)*, 2010, pp. 254–258.

[24] **A. Iqbal** and **S. Moinuddin**, "Modeling and analysis of a six-phase induction machine under fault conditions," *IEEE Trans. Ind. Appl.*, vol. 43, no. 3, pp. 730–738, May/Jun. 2007.

[25] **M. Ben Slimene**, "Performance analysis of six-phase induction machine-multilevel inverter with arbitrary displacement," *Electr. Eng. Electromech.*, no. 4, pp. 12–17, 2020.

[26] **S. X. Ding**, *Model-Based Fault Diagnosis Techniques: Design Schemes, Algorithms and Tools*, 2nd ed. London, U.K.: Springer-Verlag, 2013.

[27] **T. W. S. Chow** and **H. Z. Tan**, "HOS-based non-parametric and parametric methodologies for machine fault detection," *IEEE Trans. Ind. Electron.*, vol. 47, no. 5, pp. 1051–1059, Oct. 2000.

[28] **M. Riera-Guasp**, **J. A. Antonino-Daviu**, and **G. A. Capolino**, "Advances in electrical machine, power electronic, and drive condition monitoring and fault detection: State of the art," *IEEE Trans. Ind. Electron.*, vol. 62, no. 3, pp. 1746–1759, Mar. 2015.

[29] **T. M. Jahns** and **J. M. Miller**, "Stator and rotor coordinate transformation for modeling and control of the induction machine," *IEEE Trans. Ind. Appl.*, vol. IA-21, no. 5, pp. 1403–1412, Sep./Oct. 1985.

[30] **T. A. Lipo**, "A d–q model for six phase induction machines," in *Proc. Int. Conf. Electr. Mach. (ICEM)*, Athens, Greece, 1980, pp. 860–867.

[31] **G. K. Singh**, **K. Nam**, and **S. K. Lim**, "A simple indirect field-oriented control scheme for multiphase induction machine," *IEEE Trans. Ind. Electron.*, vol. 52, no. 4, pp. 1177–1184, Aug. 2005.

[32] **E. Jung**, **H. Yoo**, **S.-K. Sul**, **H.-S. Choi**, and **Y.-Y. Choi**, "A nine-phase permanent-magnet motor drive system for an ultrahigh-speed elevator," *IEEE Trans. Ind. Appl.*, vol. 48, no. 3, pp. 987–995, May/Jun. 2012.

[33] **M. N. Uddin**, **T. S. Radwan**, and **M. A. Rahman**, "Performance of fuzzy-logic-based indirect vector control for induction motor drive," *IEEE Trans. Ind. Appl.*, vol. 38, no. 5, pp. 1219–1225, Sep./Oct. 2002.

[34] **W. Shepherd** and **L. Zhang**, *Power Converter Circuits*. Boca Raton, FL, USA: CRC Press, 2004, ch. 11, pp. 114–116.

[35] **H. Kim** and **S.-K. Sul**, "A novel filter design for output LC filters of PWM inverters," *J. Power Electron.*, vol. 11, no. 1, pp. 74–81, Jan. 2011.

[36] **P. L. Fagundes**, **A. R. S. Santos**, and **L. A. C. Oliveira**, "Analysis and implementation of a two-level inverter for induction motor control," *IEEE Trans. Ind. Electron.*, vol. 61, no. 5, pp. 2583–2591, May 2014.

[37] **J. Holtz**, "Pulse width modulation—A survey," *IEEE Trans. Ind. Electron.*, vol. 39, no. 5, pp. 410–420, Oct. 1992.

[38] **F. Blaschke**, "The principle of field orientation as applied to the new transvector closed-loop control system for rotating-field machines," *Siemens Rev.*, vol. 34, no. 5, pp. 217–220, May 1972.

[39] **J. Holtz**, "Vector control of three-phase AC machines," *IEEE Trans. Ind. Electron.*, vol. 41, no. 5, pp. 654–662, Oct. 1994.

[40] **B. K. Bose**, *Modern Power Electronics and AC Drives*. Upper Saddle River, NJ, USA: Prentice Hall, 2002.

[41] **Bojoi, R**, *Analysis, design and implementation of a dual three-phase vector controlled induction motor drive*. Ph.D dissertation, Politecnico Di Torino, Italy, 2002.

[42] **B. K. Bose**, "Power Electronics and AC Drive", Prentice Hall. 1986.

[43] **P. Vas**, "Vector Control of AC Machines", New York, Oxford Science Publications. 1990.

[44] **W.Leonhard**, "Control of Electrical Drives", SPRINGER, 2nd Edition, 1996.

[45] **F. Blaschke**, "The principle of field oriented as applied to the new Tran vector closed-loop control system for rotating machine", Siemens Review, 1972, vol.39, N°4, pp.217-220.

[46] **K. Hasse**, "On the dynamics of speed control of a static AC drive with squirrel cage induction machine", Ph.D. Dissertation, Tech. HochschuleDarmstradt, Germany, July 1979.

Appendix

► A.1 - Parameters of the dual three-phase induction machine:

Parameters	Numerical value
Rated Power P_n	4.5 KW
Rated current I_n	6.5 A
Rated voltage V_n	220/380 V
Rated frequency f_n	50Hz
Résistances statorique R_{s1}, R_{s2}	3.72 Ω
Résistance rotorique R_r	2.12 Ω
Inductance statorique L_{s1}, L_{s2}	0.022 H
Inductance rotorique L_r	0.006H
Inductance mutuelle L_m	0.3672 H
Coefficient de frottementfv	0,001 Nm s/rd
Tension du bus continu U_{DC}	1200V
Moment d'inertie J	0.0625 kg.m^2
Nombre de paires de pôles p	1